CHARACTERIZATION OF AIR TO FUEL RATIO CONTROL AND NON-SELECTIVE CATALYTIC REDUCTION ON AN INTEGRAL COMPRESSOR ENGINE

by

KYLE MARTIN WOLFRAM

B.S., Kansas State University, 2006

A THESIS

submitted in partial fulfillment of the requirements for the degree

MASTER OF SCIENCE

Department of Mechanical and Nuclear Engineering
College of Engineering

KANSAS STATE UNIVERSITY
Manhattan, Kansas

2008

Approved by:

Major Professor
Kirby S. Chapman, Ph.D.

Abstract

In the natural gas production industry, recent legislation has mandated new emission regulations for low horsepower reciprocating internal combustion engines. One method to achieve compliance of the new regulations is the use of non-selective catalytic reduction. Non-selective catalytic reduction utilizes a three-way catalyst and an air-to-fuel ratio controller to oxidize carbon monoxide and unburned fuel while reducing oxides of nitrogen. Testing of a non-selective catalytic reduction system was preformed on a typical exploration and production engine, a Compressco GasJack. To fully test the unit, exhaust gas samples were taken with an ECOM gas analyzer both before and after the catalyst over typical engine speeds and powers. By sampling the exhaust gas concentration before and after the catalyst, the catalyst efficiency or percent reduction in exhaust gas specific concentrations were calculated. Additionally by testing throughout the engine's typical operation range, conditions under which the non-selective catalyst reduction system fails were determined. After testing, it was found that the three-way catalyst was effective at reducing oxides of nitrogen by 98% at all speeds and power conditions. Carbon monoxide was reduced by 90% under all conditions except for maximum speed and power. At maximum speed and power, the conversion efficiency for carbon monoxide was recorded as low as 32%. One reason for the low conversion efficiency at maximum speed and power was that the oxygen concentration entering the catalyst was not sufficient to oxidize the carbon monoxide to carbon dioxide. These results indicate the three-way catalyst was effective at reducing emissions when the controller correctly maintained the pre-catalyst oxygen concentration. However, the controller was unable to maintain engine operation at the ideal air-to-fuel ratio at all test conditions. The controller failed to keep the pre-catalyst oxygen concentration in the correct range because the oxygen sensor was not accurate and consistent in its output. Future work on the development of a more robust oxygen sensor is recommended.

Table of Contents

List of Figures

List of Tables

Nomenclature

Acronyms

AFR	Air-to-fuel ratio
AFRC	Air-to-fuel ratio control
AGA	American Gas Association
CDP	Compressor discharge pressure
CFR	Code of federal regulation
COV	Coefficient of variation
E&P	Exploration and production
EGO	Exhaust gas oxygen
EPA	Environmental Protection Agency
NGML	National Gas Machinery Laboratory
NMHC	Non-methane hydrocarbons
NSCR	Non-selective catalytic reduction
NSPS	New source performance standards
OEM	Original equipment manufacturer
RICE	Rich burn internal combustion engine
UBHC	Unburned hydrocarbons

Variables and Parameters

A	Area
AF	Air-to-fuel ratio
b	Bore
bdc	Bottom dead center
$bmep$	Brake mean effective pressure
$BSFC$	Brake specific fuel consumption
d	Diameter
E	Emissions

F	Faraday constant
$fmep$	Friction mean effective pressure
h	Specific enthalpy
$imep$	Indicated mean effective pressure
HHV	Fuel higher heating value
LHV	Fuel lower heating value
M	Molecular weight
$\dot{m}$	Mass flow rate
N	Rotating speed
n	Moles per mole of fuel
p	Pressure
Q	Volumetric flow rate
r	Compression ratio
R_u	Universal gas constant
s	Stroke
T	Temperature
tdc	Top dead center
V	Velocity
$\forbar{V}$	Volume
$\dot{W}$	Power
x	Mass fraction
y	Mole fraction
Y	Gas expansion coefficient
z	Hydrocarbon radical
Z	Distance

Greek variables

β	Ratio of diameters
Δ	Change in a condition, as in Δh is the change in specific enthalpy
η	Efficiency

λ	Excess air, inverse of equivalence ratio
ρ	Density
σ	Uncertainty, as in σ_x is the uncertainty in x
τ	Torque
ϕ	Equivalence ratio

Subscripts

a	Air
b	Brake
d	Displacement
D	Discharge
f	Fluid
i	i^{th} number in a set
n	Total number in a set
S	Suction
std	Standard
stoich	Stoichiometric
th	Thermal

Chemical Compounds

CH_4	Methane
$C_\alpha H_\beta O_\gamma N_\delta$	Generic Hydro-carbon fuel
CO	Carbon Monoxide
CO_2	Carbon Dioxide
H_2	Hydrogen
H_2O	Water
N_2	Nitrogen
NO	Nitric Oxide
NO_2	Nitrogen Dioxide
NO_x	Oxides of Nitrogen
O	Ozone

O_2	Oxygen
OH	Hydroxide

Acknowledgements

I would like to thank Compressco and Emit for donating equipment for this project. Compressco donated the engine and compressor skid for testing. Emit donated a three-way catalyst, an air-to-fuel ratio controller, and the necessary accessory's to get the system up and running. Both companies also were very helpful in installing the NSCR system and making sure that everything was functioning correctly.

Dedication

This work is dedicated to my wife Leah. She showed support by understanding while I spent many hours in the lab running tests as well as the time spent collecting the results and writing this thesis. It was only through her support that this thesis was completed.

CHAPTER 1 - Introduction

The goal of this project was to quantify the exhaust gas emission levels from a typical exploration and production (E&P) engine which can consistently and reliably be achieved using currently available "off the shelf" non-selective catalytic reduction (NSCR) and air-to-fuel ratio control (AFRC) technology. A database of expected emissions was built by operating the engine over typical exploration and production operating ranges and applications. Specifically a Compressco GasJack, like the one seen in Figure 1.1, rich burn internal combustion engine (RICE) and integral reciprocating compressor was installed in a laboratory environment and thoroughly tested throughout its expected operating range. The following steps were taken to achieve completion of this project:

- Install a commercially available NSCR and AFRC package;
- Test the engine's exhaust concentration before entering the catalyst;
- Test the engine's exhaust concentration after leaving the catalyst;
- Observe the performance of the engine and air-to-fuel ratio control system; and
- Record all engine and compressor operating data.

Figure 1.1 Compressco GasJack Compressor

Source: http://www.compressco.com/

Motivation

The natural gas industry is made up of three main sectors: collection, transmission, and distribution. In the collection and transmission sectors, compressors are necessary to increase the pressure of the natural gas to move it from the gas fields to homes and industries. These compressors are driven by reciprocating engines, gas turbine engines, or high speed electric motors. The reciprocating engines are widely popular and many have been around since the 1940's (Beshouri et al., 2005). One major advantage of reciprocating engines is that they are very reliable and robust. Emissions regulatory rules however, have recently become an issue for these engines. Large stationary reciprocating engines and automobile engines have been required to meet pollution criteria for carbon monoxide, oxides of nitrogen, and other combustion products since the 1970's (Tice, 2007). Recent legislation in the four corners region of Colorado, New Mexico, Utah and Arizona now require all new and rebuilt engines to meet emission standards for oxides of nitrogen (NO_x), carbon monoxide (CO) and non-methane hydrocarbons (NMHC). This legislation calls for all new emission sources to meet or exceed the environmental protection agency's new source performance standards (NSPS). Small engines with power ratings lower than 25 horsepower become subject to emission requirements detailed in 40 CFR part 90 (EPA, 2007). For larger engines the EPA breaks down emissions regulations by fuel type and horsepower rating. Table 1.1 indicates the regulations for new engines installed from 2007 through 2011.

Table 1.1 EPA New Source Performance Standards

EPA SI NSPS NPRM

NOx/CO/NMHC (g/bhp-hr)		2007		2008		2009		2010		2011	
		1-Jan	1-Jul	1-Jan	1-Jul	1-Jan	1-Jul	1-Jan	1-Jul	1-Jan	1-Jul
All engines	< 25 hp			40 CFR 90							
Gasoline & RB LPG	26-499 hp			40 CFR 1048							
	≥ 500 hp		40 CFR 1048								
Natural gas & LB LPG				40 CFR 90							
Non-emergency	26-499 hp			2.0/4.0/1.0						1.0/2.0/0.7	
	≥ 500 hp		2.0/4.0/1.0						1.0/2.0/0.7		
Emergency	> 25 hp						2.0/4.0/1.0				
Landfill / digester gas	< 500 hp			3.0/5.0/1.0						2.0/5.0/1.0	
	≥ 500 hp		3.0/5.0/1.0						2.0/5.0/1.0		

Notes: Standards do not apply to engines ordered before proposal publication date (expected to be about 6/7/06).
NG & LB LPG, 25-50 hp, may instead comply with 40 CFR 1048.
Engines ≤ 40 hp that are ≤ 1000 cc may instead comply with 40 CFR 90.

Source: Four Corners Air Quality Task Force, 2007

Specifically in the 4 corners region of Colorado, New Mexico, Utah, and Arizona a regional haze has been developing lately and a task force has been assigned to study and mitigate pollutants from E & P engines (Four Corners Air Quality Task Force, 2007).

One method that has been proposed to allow rich burn engines to meet new air quality standards is the use of non-selective catalytic reduction. Current NSCR systems are commercially available from manufacturers such as Emit and Miratech. These technologies however, have not been installed on smaller E & P engines for a significant length of time and therefore the expected emission reduction capabilities are not fully known. While expectations are that the systems will scale down and reduce emissions from these lower horsepower engines, there is not enough data to accurately predict the consistency of reduction. After completion of this project, a complete set of data will be available to determine how different engine loads and speeds affect the emissions from these retrofitted engines.

Chapter 2 documents the current state of the art in NSCR and AFRC as applied to rich burn internal combustion engines. It examines the combustion chemistry involved in an internal combustion engine and the chemical reactions which take place in a catalyst. Chapter 2 also includes a review of other NSCR experiments that have been performed on natural gas and gasoline powered engines. Chapter 3 contains the mathematical model for the experiment. This includes all calculations involved in transforming raw test data into useful information, including the Benedict Webb Rubin equation of state for the flowing compressed gas, an energy balance to determine compressor power, and useful engine performance parameters. Chapter 4 details the experimental setup at the National Gas Machinery Laboratory. Since a new test cell was installed for this engine, Chapter 4 includes information about the test cell, the instrumentation used, and the control system. Chapter 5 contains the test results, discussion, and trends developed from testing the engine. Finally the last chapter, Chapter 6 gives the conclusions and recommendations for further study.

CHAPTER 2 - Literature Review

Reciprocating Engines

Throughout the years the reciprocating engine has seen many uses, from powering almost all automobiles and ships, to driving generators for electric power generation. The reciprocating engine has proven its durability and longevity. The internal combustion piston engine was first developed in the late 1800s, and has had significant development over the last 100 years (Ferguson and Kirkpatrick, 2001). Currently there are two main cycles used in internal combustion engines, the Otto and the Diesel. Notable differences between the two cycles are the fuels, the method of combustion and the acceptable compression ratios. The cycle which is of interest in this thesis is the Otto cycle. It was invented by and named after Nikolaus Otto in the year 1876 (Heywood, 1988). The basic four strokes are intake, compression, expansion (power) and exhaust. Typically these engines have valves which are mechanically connected to the crankshaft and open and close at specific times to allow fresh intake charge and spent exhaust charge in and out of the cylinder. Figure 2.1 shows the four different strokes and the corresponding valve configuration (Ferguson and Kirkpatrick, 2001).

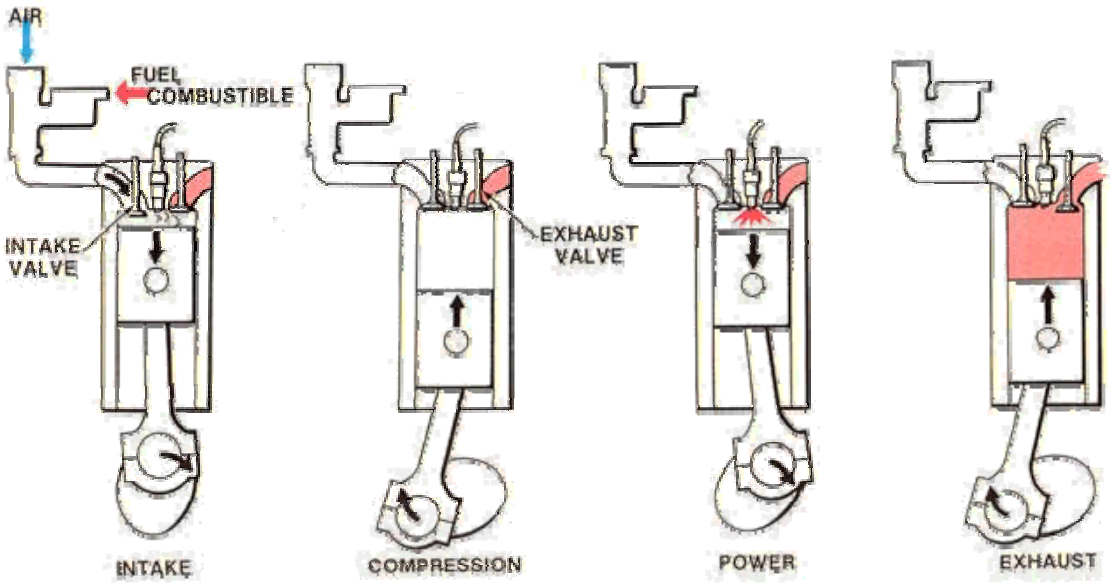

Figure 2.1 4-Stroke cycle engine

Source: http://www.amsoil.com/graphs/4_cycle_schem_640px.jpg

On the intake stroke, both air and fuel are pulled into the cylinder by a negative pressure gradient created when the piston moves downward in Figure 2.1. This fuel and air mixture is next compressed by the piston moving upward while the valves are all closed. Next the spark plug ignites the compressed fuel air mixture and it rapidly expands forcing the piston down. The piston is connected to a crankshaft by a connecting rod, and the expansion stroke creates the rotating mechanical power for the crankshaft. Finally, the piston moves back up with the exhaust valve open to discharge the spent air and fuel (Ferguson and Kirkpatrick, 2001).

During the power stroke the intake charge is ignited and the manner in which it burns depends on the mass ratio of air to fuel (Heywood, 1988). A stoichiometric mixture is defined as exactly enough air mass to completely combust the fuel mass. The stoichiometric air-to-fuel ratio depends on the fuel because different fuels have different molecular weights. Natural gas is often made up of over 90% methane, and because of this it is often modeled as pure methane for simplicity. An example of the combustion reaction for methane which occurs in an engine is give in equation (2.1).

$$CH_4 + 2\left(O_2 + 3.76N_2\right) \rightarrow CO_2 + 2H_2O + N_2 \tag{2.1}$$

The equation is balanced with the theoretical amount of air for complete combustion. After balancing the atoms in equation (2.1), the stoichiometric air-to-fuel ratio is determined by (Moran and Shapiro, 2004):

$$AF_{stoich} = \frac{2M_{O_2} + 2\times 3.76M_{N_2}}{M_C + 4M_H} = \frac{2\times 32 + 2\times 3.76\times 28.01}{12.01 + 4\times 1.008} = 17.191 \tag{2.2}$$

Next, by introducing an excess amount of air into the previously balanced combustion reaction of equation (2.1), the air-to-fuel ratio can be changed to something other than the stoichiometric air-to-fuel ratio. Equation (2.3) shows twice the amount of theoretical air, which is called 100% excess air (Moran and Shapiro, 2004).

$$CH_4 + 2\cdot 2\left(O_2 + 3.76N_2\right) \rightarrow CO_2 + 2H_2O + 15N_2 + 2O_2 \tag{2.3}$$

The air-to-fuel ratio can again be calculated by equation (2.4).

$$AF = \frac{2\times 2M_{O_2} + 2\times 2\times 3.76M_{N_2}}{M_C + 4M_H} = \frac{2\times 2\times 32 + 2\times 2\times 3.76\times 28.01}{12.01 + 4\times 1.008} = 34.383 \tag{2.4}$$

The equivalence ratio is used to normalize the air-to-fuel ratio. When comparing equivalence ratios, a value of less than one indicates lean combustion. For lean combustion there is more than the theoretical amount of air is supplied to the engine. An equivalence ratio of greater than one indicates rich combustion and means there is not enough air to fully combust the

fuel. Finally a value of one indicates there is exactly enough air and fuel for complete combustion (Heywood, 1988). The equivalence ratio is defined as:

$$\phi = \frac{AF_{stoich}}{AF} \tag{2.5}$$

When using the above example of combustion with 100% excess air, the equivalence ratio would be:

$$\phi = \frac{AF_{stoich}}{AF} = \frac{17.191}{34.383} = 0.50 \tag{2.6}$$

The equivalence ratio is useful in characterizing whether engines are lean or rich burn engines (Moran and Shapiro, 2004). Lean burn engines are those that run at AFRs greater than the stoichiometric mixture (i.e. equivalence ratios less than 1.0); however there is still debate on exactly what is a rich burn engine. The Reciprocating Internal Combustion Engine Work Group has made a case for several different definitions (Reciprocating Internal Combustion Engine Work Group of the Industrial Combustion Coordinated Rulemaking, 1998). The following is a list of their possible definitions for a rich burn engine.

- Defined by the manufacturer as rich burn
- Engine capable of using NSCR
- Engine which operates near stoichiometric conditions
- Engine where the AFR divided by the stoichiometric AFR is 1.1 or less
- Engine with 4% or less O_2 content in the exhaust
- Engine with 1% or less O_2 content in the exhaust

After the study, it was agreed that engines operating with AFRs less than the stoichiometric AFR are rich burn engines, as well as engines with 0.5% oxygen or less in the exhaust stream. A case can still be made for the other definitions, but for the rest of this document a rich burn engine is one that follows the above definitions agreed upon by the Reciprocating Internal Combustion Engine Work Group.(Reciprocating Internal Combustion Engine Work Group of the Industrial Combustion Coordinated Rulemaking, 1998).

In addition to the equivalence ratio, other parameters are necessary when studying a reciprocating engine. The performance of an internal combustion engine is typically defined by several universal parameters. Table 2.1 lists some of the most common geometrical and operational parameters for engine testing.

Table 2.1 Internal Combustion Engine Parameters

b	Bore	Piston diameter
s	Stroke	Distance piston travels in cylinder
V_d	Displacement Volume	$\frac{\pi}{4}b^2 s$
r	Compression Ratio	$\frac{V_{bdc}}{V_{tdc}}$
N	Rotating Speed	Engine revolution frequency
$\dot{W}_b$	Brake Power	$2\pi\tau N$
$bmep$	Brake Mean Effective Pressure	$\frac{2\dot{W}_b}{V_d N}$
$imep$	Indicate Mean Effective Pressure	$\frac{\int pdV}{V_d}$
$fmep$	Friction Mean Effective Pressure	$imep - bmep$
$BSFC$	Brake Specific Fuel Consumption	$\frac{\dot{m}_f}{\dot{W}_b}$
η_{th}	Thermal Efficiency	$\frac{\dot{W}_b}{\dot{m}_f LHV}$

The bore is the diameter of the piston, and the stroke is the distance from top dead center (tdc) to bottom dead center (bdc), or the distance the piston moves. By multiplying the circular bore area by the stroke, the displacement volume of the engine is calculated. Engine speed is measured in revolutions per minute (rpm) and is a measure of the rotating frequency of the crankshaft within the engine. Brake power is the rate at which work is performed by the engine. It is typically calculated after measuring the engine torque with a dynamometer (Ferguson and

Kirkpatrick, 2001). Brake mean effective pressure (bmep) is a useful engine performance parameter which is obtained by dividing the work performed by the displacement volume over a cycle (Heywood, 1988). Indicated mean effective pressure (imep) is the due to the work the gas does on the piston. In engine testing, the integral of pressure over the change in volume is calculated from a pressure trace obtained with a high speed pressure sensor. After the bmep and imep are calculated, the friction mean effective pressure (fmep) can be found. The fmep is a good measure of the frictional losses in the engine. To determine the thermal efficiency of an engine, the brake power, fuel flow rate and lower heating value are needed (Ferguson and Kirkpatrick, 2001). The detailed equations to find these parameters as they apply to testing for this thesis are discussed in Chapter 3.

Internal combustion reciprocating engines have both advantages and disadvantages for use in the gas production industry. An obvious benefit of the reciprocating engine is its durability. As stated earlier, internal combustion engines have been around for over 100 years. They are very well understood, and there is a large labor force of designers and mechanics to keep them running for years to come (Heywood, 1988). Another benefit is that they can burn the raw natural gas that they are producing; this allows them to run continuously in remote locations with little or no operator intervention. One disadvantage of using an internal combustion engine is that they typically have lower efficiency and higher emission than a comparably sized gas turbine (Bathie, 1996). Emissions are created during combustion in several different ways, therefore a careful look at pollutant formation in necessary.

Pollutant Formation

Internal combustion reciprocating engines are one source of air pollution (Heywood, 1988). Both automobiles and stationary engines contribute to the formation of trace quantities of harmful gases such as the oxides of nitrogen, carbon monoxide and unburned hydrocarbons. The actual concentrations of NO_x and CO are generally different than what would be predicted from chemical equilibrium due to the complex chemical mechanisms by which the compounds are formed (Heywood, 1988). Figure 2.2 shows how the pollution compounds are formed in a typical spark ignition engine.

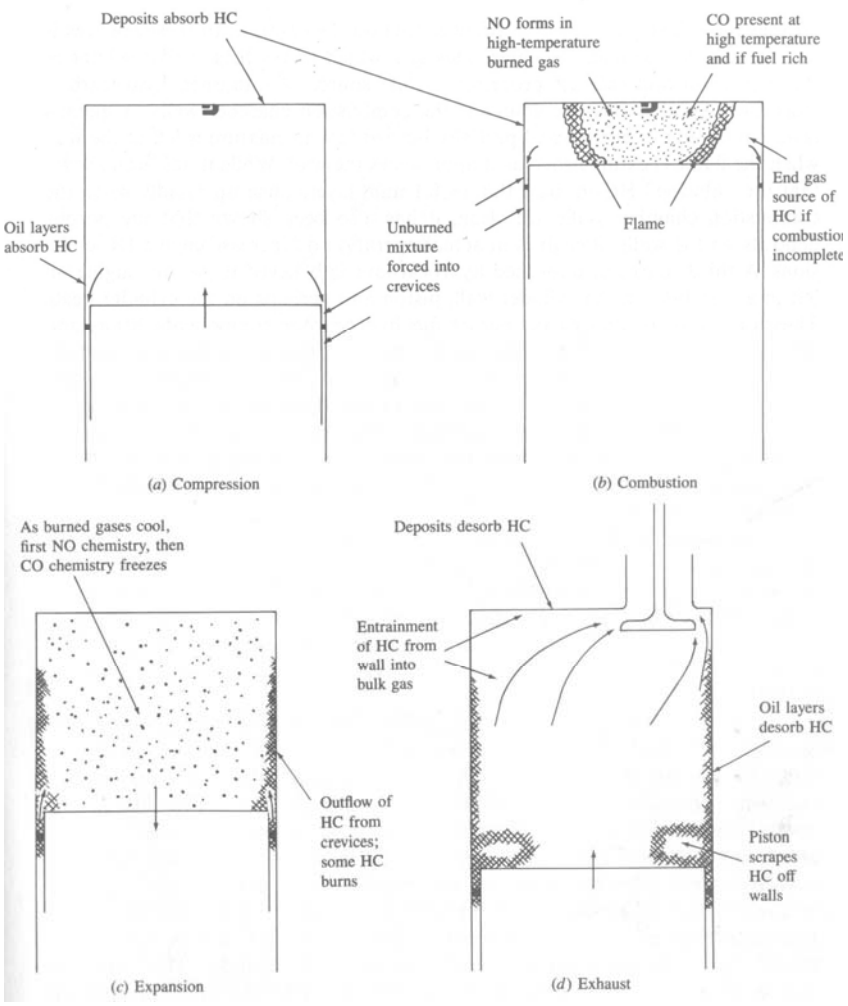

Figure 2.2 Pollution Formation During Combustion

Source: Heywood, 1988

During the compression stroke, the fuel and air mixture is absorbed into a layer of oil on the cylinder wall and fills in the crevice around the piston down to the top ring. These two actions are a major source of the unburned hydrocarbons found in an engine's exhaust stream (Heywood, 1988). At the end of the compression stroke, typically a few crank angle degrees before the piston reaches top dead center, the spark plug fires and starts a combustion wave or flame which travels away from the spark plug downward towards the piston starting the expansion or power stroke (Ferguson and Kirkpatrick, 2001). At that instant, the chemical reactions which take place are responsible for forming NO and CO. NO form due to high temperatures in the combusted gases following the flame wave. CO forms at the flame when there is not enough oxygen present for the carbon to fully react to form CO_2. Next, the piston

moves down expanding the gases which causes rapid cooling. This cooling process freezes the NO and CO which were created at combustion. After the expansion, the harmful pollutants are now formed and change very little from this point unless some exhaust gas after treatment system is used (Heywood, 1988).

NO formation in internal combustion engines has been widely studied and under rich burn conditions, the governing equations by which NO are formed during combustion are collectively called the Zeldovich mechanism:

$$O + N_2 \rightarrow NO + N \tag{2.7}$$

$$N + O_2 \rightarrow NO + O \tag{2.8}$$

$$N + OH \rightarrow NO + H \tag{2.9}$$

$$NO + HO_2 \rightarrow NO_2 + OH \tag{2.10}$$

NO is the compound formed as a direct result of combustion when temperatures are above 3140°F (Agrawal et al., 2004). The concentration of NO is dependent on both temperature and time spent at that temperature. Exhaust gas also contains NO_2 in addition to the NO. In a rich burn spark ignition engine, NO_2 is formed through the reaction in equation (2.10). The NO_2 is created after combustion in the exhaust stream and the ratio of NO_2 to NO is typically very small (Heywood, 1988). However, when testing emissions both NO and NO_2 are grouped together and thought of as NO_x.

CO emissions in an internal combustion engine are highly dependent on the air-to-fuel ratio (Heywood, 1988). CO is a direct result from one of the principal chain reactions as hydrocarbons are oxidized into CO_2 and H_2O.

$$zH \rightarrow z \rightarrow zO_2 \rightarrow zCHO \rightarrow zCO \rightarrow CO \tag{2.11}$$

$$CO + OH \rightarrow CO_2 + H \tag{2.12}$$

Equation (2.11) shows the chain reaction of the oxidation of hydrocarbons where *z* is the hydrocarbon radical, the ratio of hydrogen to carbon atoms in the fuel. Equation (2.12) continues the reaction from CO to CO_2, however this reaction is slower than reaction (2.11) and if the air-to-fuel ratio is rich, expansion freezes the CO before reaction (2.12) can take place causing CO to be found in the exhaust (Heywood, 1988).

Air Quality Act

The air quality act was passed by the United States Congress in 1967 (Rowell, 2007). Although it required no actual standards, it was a sign that emissions concerns were becoming

realized. In 1970, congress passed the clean air act. The clean air act had three components. First the EPA was to identify and regulate carbon monoxide (CO), nitrogen dioxide (NO_2), ozone (O), sulfur dioxide (SO_2), particulate matter less than 10 micrometers (PM-10), and lead. The second component was to identify primary and secondary standards. Primary standards protect the health of the public and secondary standards protect the environment. The third component of the clean air act was the phasing out of lead-based gasoline (Rowell, 2007). The clean air act has undergone amendments in 1977 and 1990 to further improve the quality of air today (Lambert, 1995). Additionally, states have enacted similar legislation to combat localized heavy pollution zones (Rowell, 2007).

By 1976 automobile makers began to use catalysts on their engines to control emissions. This was only becoming a possibility as the lead was removed from gasoline (Rowell, 2007). In the early days of catalyst use, cars lacked power, were hard to start, and generally did not perform well. To improve automobile performance engineers worked extensively with the onboard computer and exhaust gas oxygen (EGO) sensors. It was found that the solution to both low emissions and good performance depended on a robust control system. By 1981 electronic fuel injection that was controlled by a computer based on feedback from the exhaust gas oxygen sensor was standard on almost all cars. This system allowed gasoline engine performance to improve substantially however, the process took five years at a minimum for completion (Tice, 2007). In the late 1980's California began implementing very restrictive NO_x emissions on large stationary natural gas engines. A process that took over five years for successful completion in the automobile industry was required of the gas industry almost overnight. Again meeting both power requirements as well as emissions requirements became a struggle. The adaptation of NSCR onto gas engines failed in many circumstances because of inconsistent fuels and the air-to-fuel ratio controller inability to handle changing ambient conditions and varying loads (Southern California Gas Company, 2007). Recently legislation was passed to regulate new installations of stationary spark ignition engines (EPA, 2007). To successfully adapt NSCR technology to these engines, it will take some time to fully address and overcome the new challenges brought on by stricter regulation.

Air-to-Fuel Ratio Control

As stated earlier, the air-to-fuel ratio which the engine is operating at can greatly affect the operating parameters of the engine. It can affect power and performance, but more so it affects the emissions created during the combustion process. The mechanism by which an engine receives fuel and air is either by a carburetor or throttle body and fuel injectors. While the throttle body and fuel injectors are a common feature on modern automobiles, the many of stationary engines operating in the natural gas collection industry are older and still utilize a carburetor (Beshouri et al., 2005). A disadvantage of the carburetor is that the fuel air mixture is set mechanically typically by an adjustment screw or some other similar method. While this can be accurately done by skilled technicians for a single load and speed, there is no system for real time adjustment of the AFR. Therefore, when the load, speed, or environmental conditions change, the AFR will vary (Lambert, 1995). This constant variation of the AFR is called an uncontrolled engine. Figure 2.3 shows how the excess air supplied to internal combustion engine affects exhaust gas concentrations of NO_x, CO and O_2.

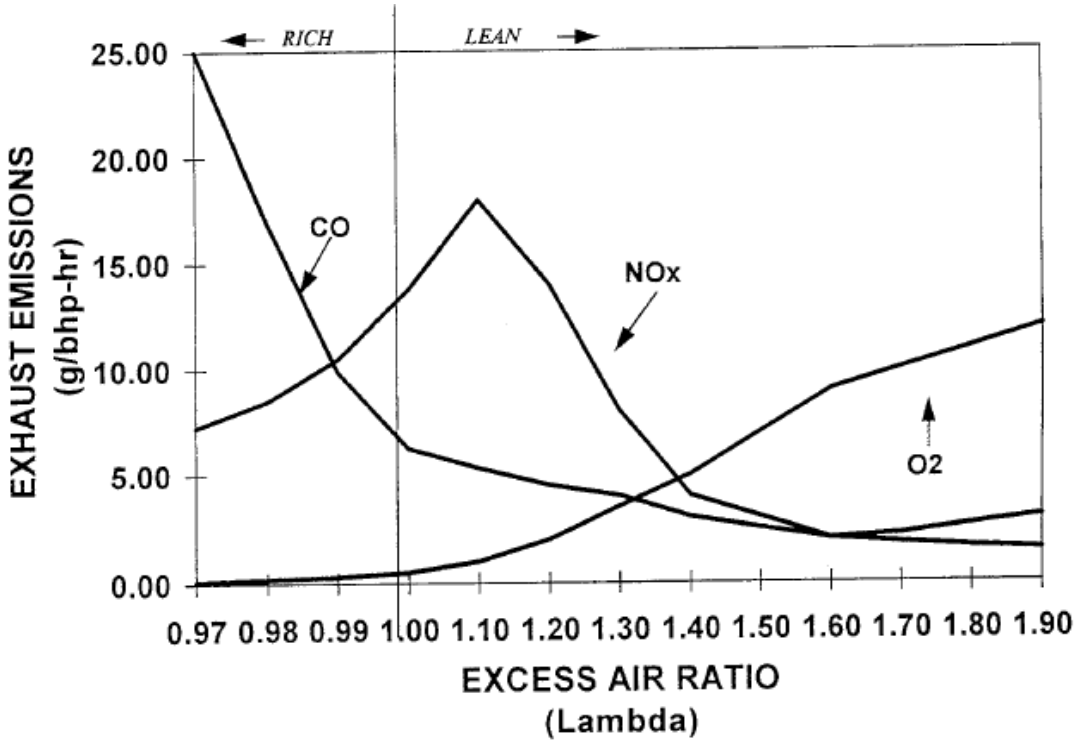

Figure 2.3 Excess Air and Exhaust Gas Composition

Source: Lambert, 1995

As seen in the figure, the amount of each exhaust species is strongly correlated to excess air. Recall that the excess air is the amount of extra air supplied beyond the theoretical amount required for stoichiometric combustion. If the excess air is uncontrolled and varying, the AFR will be uncontrolled and changing as well. Precisely controlling the AFR is the first step to reducing emissions without sacrificing power (Tice, 2007). To bring the engine under control, an engine can be retrofitted with an air-to-fuel ratio controller (Kennedy and Holdeman, 2006).

Air-to-fuel ratio controllers work by adjusting the fuel flow rate based on the oxygen content measured in the exhaust stream (Ciulla, 2003). An EGO sensor is installed in the exhaust pipe near the engine. Exhaust gas oxygen sensors contain a zirconium oxide element that is sensitive to oxygen levels (Ferguson and Kirkpatrick, 2001). The sensor typically creates a voltage between 0 and 1,000 mV depending on the oxygen content in the exhaust. Figure 2.4 shows the typical relationship between the EGO voltage output and the equivalence ratio.

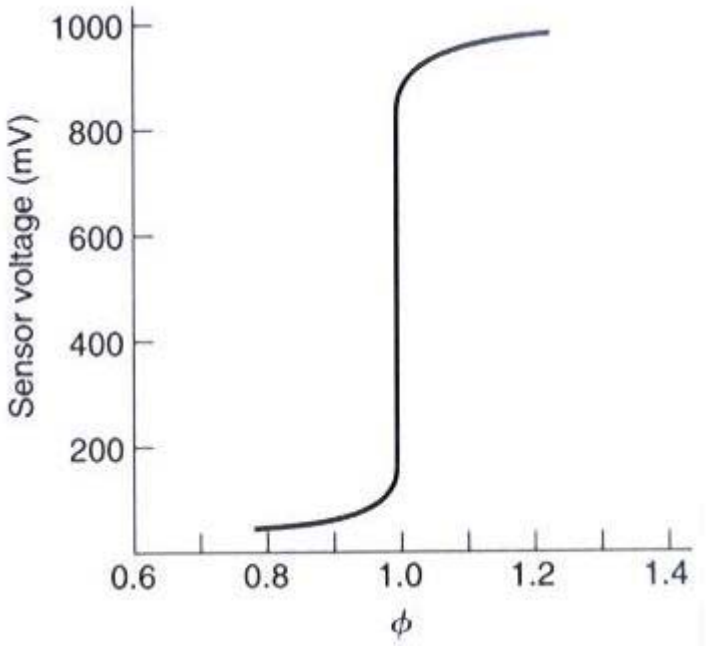

Figure 2.4 Lambda Sensor Curve

Source: Ferguson & Kirkpatrick, 2001

The sensor is very sensitive and non-linear near stoichiometric combustion with large changes in the output between slightly lean and slightly rich conditions (Ferguson and Kirkpatrick, 2001). The oxygen sensor output is ideally predicted by the Nernst equation.

$$V_o = \frac{R_u T}{4F} \ln\left(\frac{P_{O_2 atm}}{P_{O_2 exhaust}}\right) \tag{2.13}$$

The parameter R_u is the ideal gas constant, T is temperature and F is the Faraday constant (F=96,484 C/mol). Due to the nature of the function, lean of stoichiometric conditions gives a voltage of 50 mV and rich conditions give an output above 800 mV (Ferguson and Kirkpatrick, 2001).

Prior to the installation of an AFRC system, an engine cannot control air and fuel flow rates independent of each other. However the AFRC adds a control valve on the fuel inlet line which adds an additional degree of freedom to alter the amount of fuel for a given flow rate of air (Kennedy and Holdeman, 2006). A simplified schematic of such a system is shown in Figure 2.5.

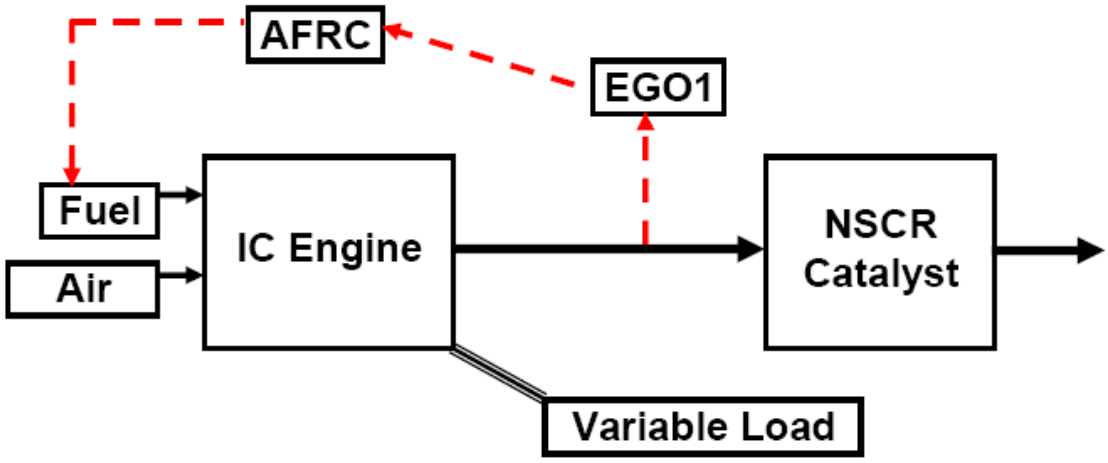

Figure 2.5 Air-to-Fuel Ratio Control System

Southern California Gas Company, 2007)

It can be seen from the figure that the system itself is mechanically simple. However, with a variable load the precision of the closed loop control system becomes the item of interest. As stated earlier as the load changes, the AFR will change correspondingly. The AFRC must be able to quickly adjust the fuel to keep the engine operating at the desired set point (Southern California Gas Company, 2007).

To determine the desired set point, testing has been done with an AFRC and NSCR system to find what AFR yields the lowest emissions. By using non-selective catalytic

reduction, CO can be oxidized to CO_2 and NO_x can be reduced to elemental N_2. However, the NSCR reactions only take place under very precise exhaust stream conditions. For example, the oxygen content in the exhaust stream must be between 0.2% and 0.7% for the reactions to occur (Kennedy and Holdeman, 2006). However, due to the difference in each oxygen sensor and each engine, the AFRC set point will vary from one engine to the next. Therefore the desired AFRC set point is obtained by altering it until the catalyst is most effective reducing both NO_x and CO (Emit Technologies, 2007).

Figure 2.6 shows the conversion efficiency of a typical NSCR system. Especially of note in the figure is the "Catalyst Window."

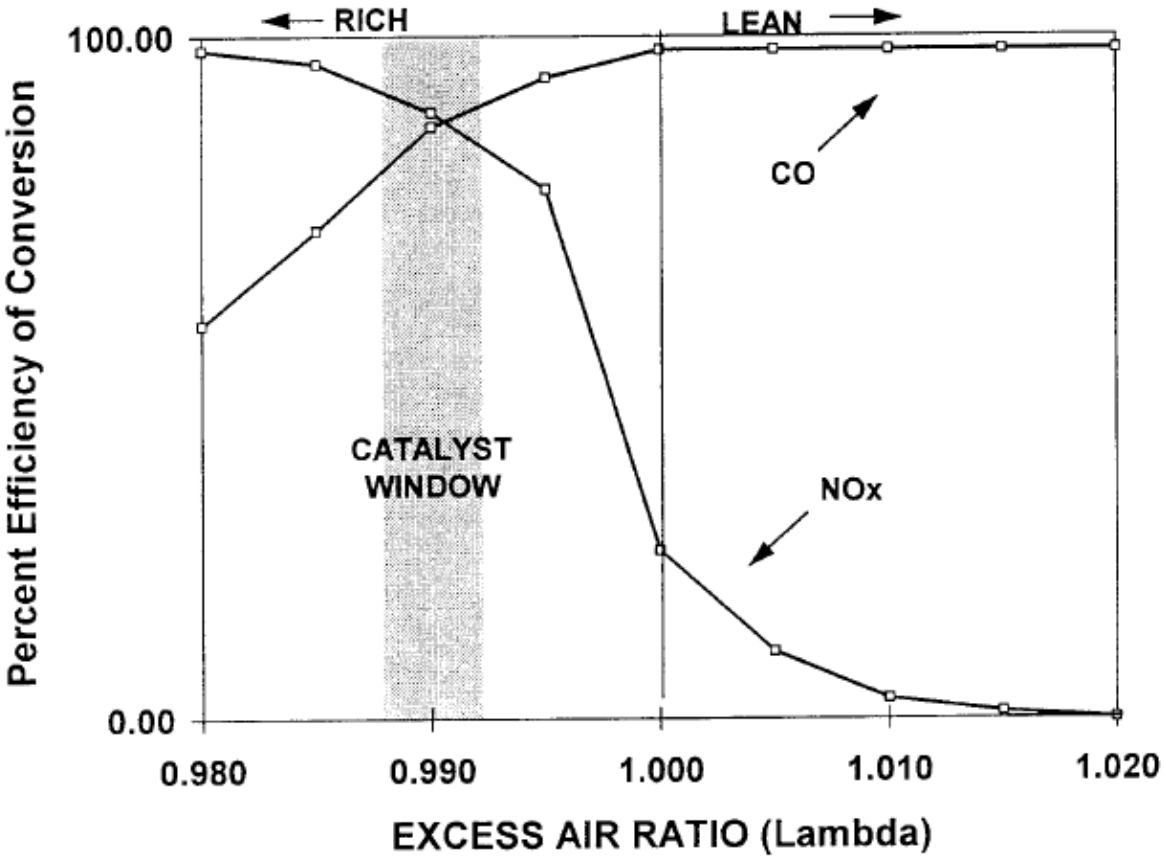

Figure 2.6 Efficiency of a Catalyst Based on Excess Air

Source: Lambert, 1995

This is the range or window that the AFRC must keep the engine operating within for a high conversion efficiency of both CO and NO_x. As seen from the figure this window is not very large, it shows that the window is λ=0.99 with a range of plus or minus 0.0025. If the engine operates outside of the window to the rich side, NO_x will be reduced significantly, while CO is

not well converted. Conversely if the engine operates on the lean side of the window, CO emissions will be lessened, while NO_x conversion efficiency drops off sharply (Lambert, 1995).

Derfoort et al. (2004) conducted a test of a three-way catalyst with air-to-fuel ratio control to determine the size of the catalyst window for 80% NO_x and CO removal on a Superior 6G-825 engine. They found that the window was an equivalence ratio of 1.013 to 1.027, with a maximum removal of 95% for both species at 1.014. This shows that very tight control of the equivalence ratio is necessary for even 80% efficiency. For the highest reduction levels, the window becomes non-existent, and instead the engine must operate at exactly the correct point (Defoort et al., 2004). While the exact figures for the window of control will vary from one engine to another, the main idea is that very tight control of the AFR is necessary for the catalyst to enhance the oxidation of CO and reduction of NO_x effectively.

All previous discussion has been focused on steady-state AFRC. This type of control works to keep the engine operating at exactly the same AFR at all times. This is by far the most common type of control (Defoort et al., 2004). However, there is another method of control called forced dithering. Forced controller dithering is the process of purposefully varying the AFRC set point to combat natural catalyst dithering. Dithering occurs naturally in a three-way catalyst. When dithering occurs, the catalyst stores then releases oxygen. This causes post-catalyst concentration of CO and NO_x to fluctuate with time as the concentration of oxygen in the catalyst changes (Arney et al., 2007). By forcing the controller to dither in the correct magnitude and period, the natural dithering of the catalyst can be reduced. When the engine runs lean, excess O_2 in the exhaust stream will oxidize CO and the catalyst will store oxygen as the NO_x is reduced. When the engine runs rich, a lack of O_2 in the exhaust will cause NO_x to be reduced as the catalyst releases O_2 to oxidize the CO (Defoort et al., 2004). This method is also called pulse width modulation. An example of how it might be set is shown in Figure 2.7. The width, frequency and wave type can be varied to best match the natural dithering in the catalyst. It has been found that the length of time on the leaner side of the mean should be longer than the time on the richer side of the mean for best results (Arney et al., 2007).

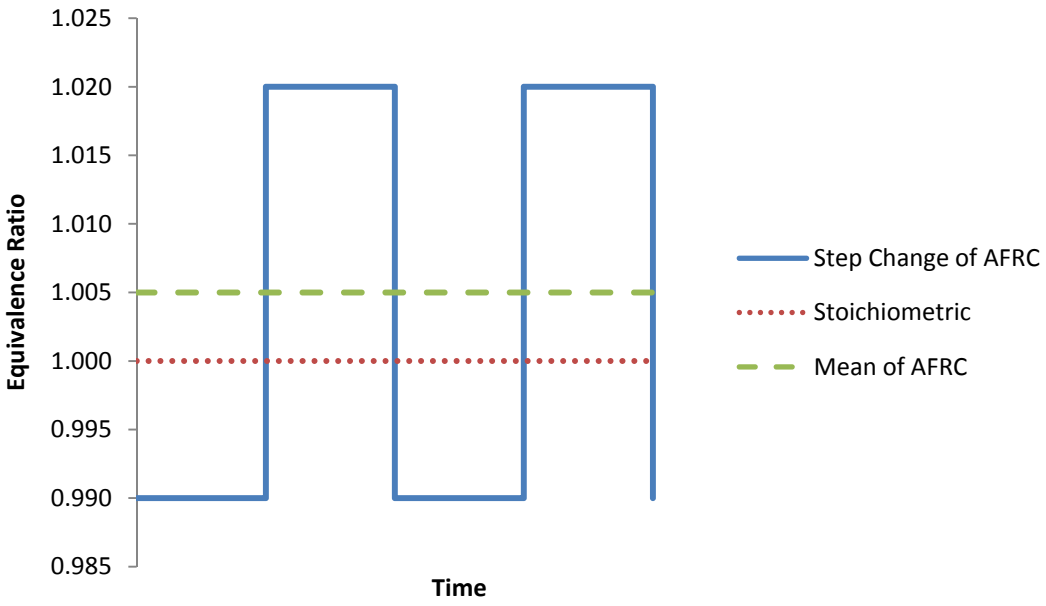

Figure 2.7 Forced Controller Dithering

In further testing by Defoort et al. (2004), it was found that 2.5 seconds leaner followed by 2.5 seconds richer with amplitude of 20% yielded the best results. The mean was an equivalence ratio of 1.014 with excursions of +/-0.01. The forced dithering of the controller lowered the maximum possible reduction from 95% to 90%, however the window of control was increased from a range of 1.013-1.027 to a slightly broader range of 1.010 to 1.030 (Defoort et al., 2004).

One common failure mode of AFRC systems has been identified by Arney et al. (2007): "A subtle shift in the operating point of the AFRC system has been noticed, which causes emissions to also slowly drift higher. The complex failure modes of the system are not identifiable by current AFRCs." This is further explored in the next section on NSCR and during the testing phase.

Non-Selective Catalytic Reduction

Non Selective Catalytic Reduction or NSCR technology consists of a new exhaust system which contains a catalyst such as platinum or palladium on a honeycomb structure (Ciulla, 2003). The catalyst promotes a positive chemical reaction to remove pollution in three ways. In the catalyst CO and unburned hydrocarbons are oxidized while NO_x is reduced. For the catalyst

to function, an oxygen sensor with closed loop control is required to precisely monitor and control the AFR. By accurately controlling the oxygen content in the exhaust to less than 0.5% by volume, up to 98% of the NO_x and CO can be converted to nitrogen, oxygen and carbon dioxide (Lambert, 1995). When the engine is running at this slightly rich of stoichiometric condition, a three-way catalytic system reduces emissions in three ways. Mathematically described as equation (2.14) oxides of nitrogen are reduced to nitrogen and oxygen. The next reaction, shown in equation (2.15) is the oxidation of carbon monoxide to carbon dioxide. The third reaction, equation (2.16), is the oxidation of unburned hydrocarbons into carbon dioxide and water vapor.

$$2NO_x \longrightarrow xO_2 + N_2 \tag{2.14}$$

$$2CO + O_2 \longrightarrow 2CO_2 \tag{2.15}$$

$$2C_xH_y + (x+y)O_2 \longrightarrow 2xCO_2 + yH_2O \tag{2.16}$$

Because of these three reactions, NSCR is often called a three-way catalyst. The term non-selective comes about because the catalyst does not have a preference to any one of the reactions over the others. This makes the NSCR system very favorable because it is capable of removing these three regulated pollutants from the exhaust stream, where as other emissions reduction strategies might reduce NO_x at the cost of increasing CO (3-Way Non-Selective Catalytic Reduction (NSCR) deNO_x Catalyst, 2007) .

NSCR is used on rich burn engines and is effective only when used with an air-to-fuel ratio controller. This is because of the precise mixture that must go into the catalyst for the positive reactions to take place. By taking a closer look at the chemistry that is involved in a successful NSCR system it is possible to determine why the mixture must be so precise for the favorable reactions to take place. The first thing to examine is the combustion reaction given in equation (2.17).

$$CH_4 + (O_2 + 3.76N_2) \longrightarrow CO_2 + H_2O + N_2 + O_2 + NO + CO + ... \tag{2.17}$$

In this case it is assumed that methane is the fuel and air is made solely of oxygen and nitrogen. After combustion, the compounds carbon monoxide (CO), carbon dioxide (CO_2), nitric oxide (NO) and a few other compounds as well as the elements oxygen (O_2) and nitrogen (N_2) remain.

The reason a catalyst makes the favorable reactions in equation (2.14) through equation (2.16) happen is that the material in the catalyst lowers the activation energy required for the

positive reactions to take place (Tice, 2007). The catalyst pulls the NO bond apart leaving free N and O atoms. The free N atoms join in pairs and form elemental N_2 and the free O atoms join to the CO creating CO_2. By inspection it can be seen that there must be enough oxygen present in the exhaust gas entering the catalyst to oxidize the CO. However, if there is too much oxygen the washcoat in the catalyst becomes coated with oxygen and the NO_x reduction is blocked from occurring. This is why the AFRC is crucial to the success of the NSCR system (Tice, 2007).

A more detailed look at the catalyst is shown in Figure 2.8. The substrate is typically a ceramic or metallic material capable of withstanding high temperatures. On the inside of the substrate a washcoat is applied in a honeycomb structure (Ciulla, 2003). The washcoat is typically an aluminum oxygen material. The washcoat can store and release oxygen so that the favorable reactions have the correct amount of oxygen content to take place. This allows for a slightly larger range of acceptable oxygen percentages entering the catalyst. If the engine runs rich, the oxygen content in the exhaust gas lessens and the washcoat releases oxygen for a short time while the AFRC brings the engine back to the desired operating air-to-fuel ratio (Tice, 2007).

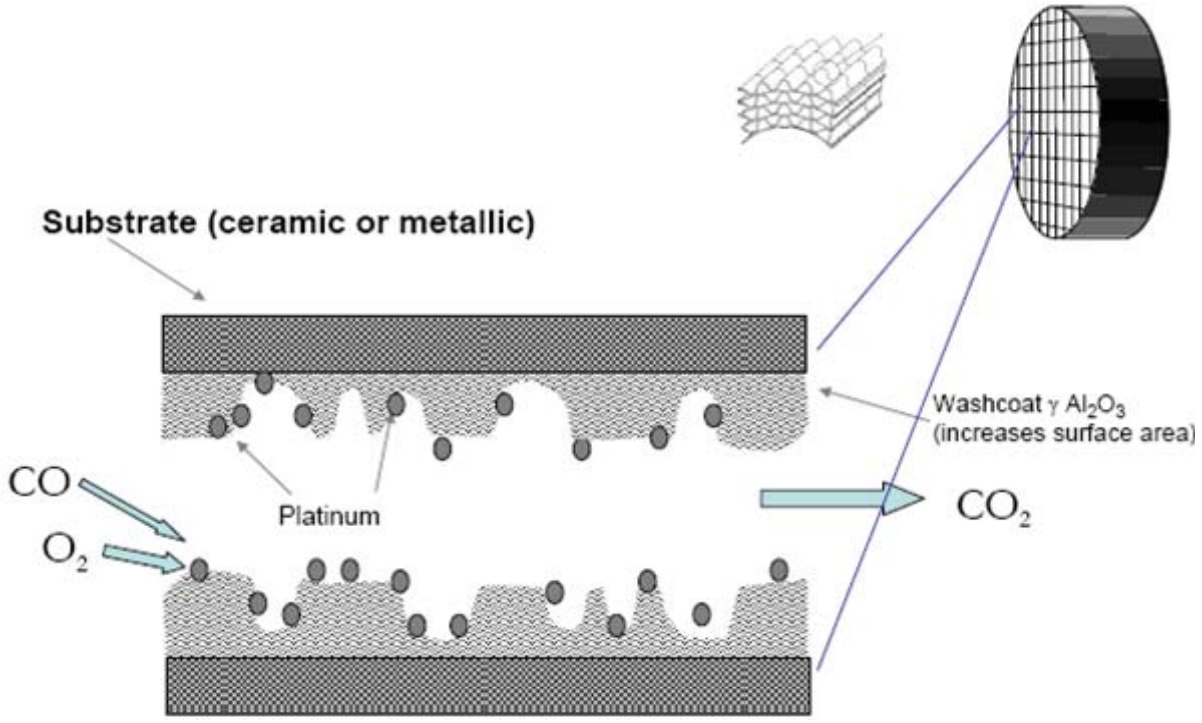

Figure 2.8 Catalyst Construction

Source: Tice, 2007

Failure modes of NSCR

NSCR systems are costly to install, and require periodic maintenance to function correctly. The high cost associated with a NSCR system along with the high likely hood of failure associated with improper use operating has created a resistance among engine users to embrace NSCR technology (Beshouri et al., 2005).

There are several types of failure modes or ways a catalyst can become poisoned causing it to stop working. The first is mechanical deactivation. This occurs when the washcoat on the catalyst is physically lost. It might break lose due to mechanical stress, vibration or thermal stress causing separation of the washcoat from the substrate. A second mode of failure is called poisoning. Figure 2.9 shows both sulfur and phosphorus poisoning (Tice, 2007).

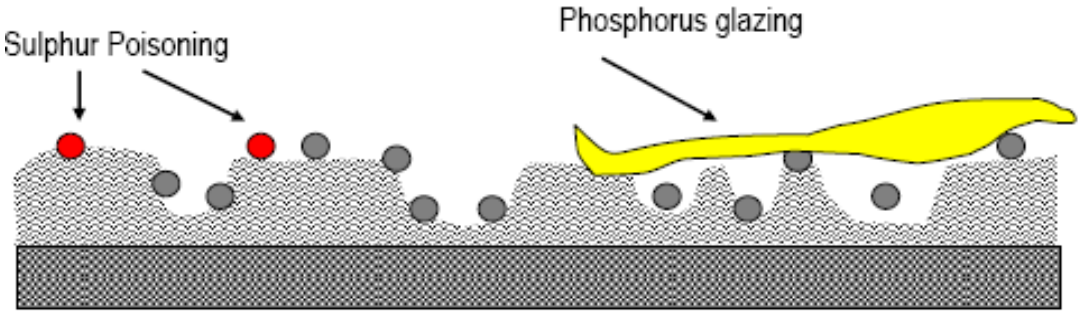

Figure 2.9 Catalyst Poisoning

Source: Tice, 2007

Catalyst poisoning occurs mainly due to sulfur in the fuel or excessive oil consumption in the engine. When high sulfur fuels are used, sulfur deposits can form on the washcoat disallowing the buildup and release of oxygen, reducing the effectiveness of the catalyst. Sulfur poisoning is reversible. It requires high temperatures and removal from the engine for cleaning. When an engine consumes a large amount of oil, either because of worn rings or other causes, phosphorus poisoning occurs. This type of poisoning is irreversible and can ruin a catalyst. The washcoat glazes over blocking the catalyst from the exhaust gas, stopping the oxidation and reduction chemical reactions from occurring (Tice, 2007).

The final common failure mode of a catalyst is thermal deactivation. This occurs when extremely high temperatures occur in the catalyst and the washcoat melts. The washcoat glazes over and encapsulates the oxygen storages zones. Figure 2.10 shows this type of failure which ruins the catalyst (Tice, 2007).

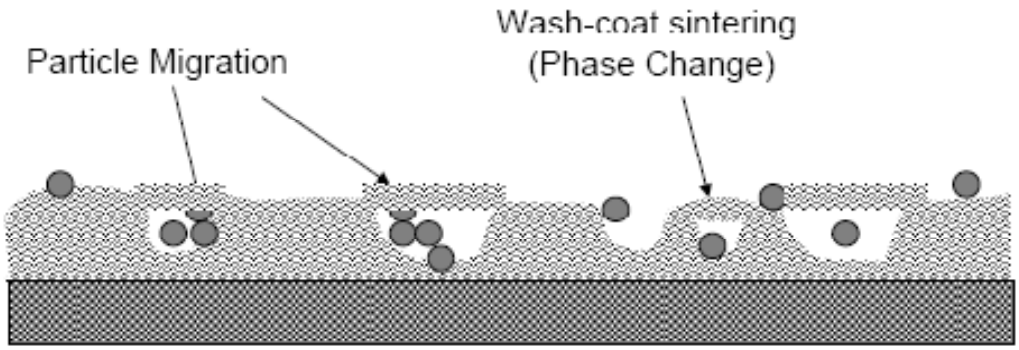

Figure 2.10 Catalyst Thermal Deactivation

Source: Tice, 2007

NSCR technology has been used with some success in automobiles and chemical plants for the past 30 years (3-Way Non-Selective Catalytic Reduction (NSCR) deNO_x Catalyst, 2007) . By carefully controlling the AFRC and NSCR systems and performing routine maintenance on the systems, these main failure modes of NSCR can be avoided (Tice, 2007). Even though non-selective catalytic reduction technologies have many advantages associated with reducing emissions, they do have drawbacks. The most dominant drawback is the possible formation of ammonia in the catalyst under rich engine condition (Chapman, 2007). While this is not yet a regulated emission, it is expected that new regulations will soon include ammonia.

In addition to having an accurate air-to-fuel ratio, other parameters, such as exhaust gas temperature and pre-catalyst emission concentrations must be in tolerable ranges to make NSCR success a possibility. According to NSCR system manufacturer Johnson and Matthey, the exhaust gas temperature should be in the range of 800 to 1,200°F and natural gas fuel should contain sulfur levels of less than 200 ppmv. The exhaust concentrations of NO_x, CO, and UBHC also need to be within tolerable ranges prior to catalytic reduction for the NSCR to be effective. NO_x levels should be between 2,000 and 4,000 ppmv, CO ranges should fall between 3,000 and 6,000 ppmv and, UBHC levels should not exceed 2000 ppmv. To avoid poisoning, the lube oil used in the engine compressor should have a consumption rate less than 0.0015 lb/hp-hr and should contain less that 0.5% sulfated ash by weight (3-Way Non-Selective Catalytic Reduction (NSCR) deNO_x Catalyst, 2007).

While NSCR and AFRC have proven successful on applications, such as automobiles, there will likely some unknown problems to be encountered with application of the technology to stationary natural gas engines.

Natural Gas Compressors

Due to the constraints of the engine, the compressor was used as the dynamometer. So while the focus of this report is on engines, a brief overview of the compressor the engine drives is necessary. Different types of compressors are usually better for a certain application than others. Some require multiple stages to achieve a high pressure ratio, and others can achieve high pressure ratios with a single stage. Therefore the application usually dictates the type of compressor that is the most useful. An overview of some popular types is given below and then a more detailed look at the reciprocating compressor is taken because it is used in the experiment performed.

The axial flow compressor spins and moves air along the same axis. Air is pulled in by the rotors, and then redirected by the stators. Rotors are connected to the rotating shaft and provide the power to move the air, while stators are stationary. One rotor and one stator make up a single stage. This compressor must be staged to achieve high pressure ratios, however since flow is axial, staging is easily achieved. This compressor is commonly used in gas turbine engines where the compressor is powered by a turbine. The advantages of this compressor design are small frontal area for a given mass flow rate, suitable for multistage, and high efficiency. While this compressor has advantages, due to the design of the axial compressor it is better suited for applications other than natural gas collection and transmission (Bathie, 1996).

A centrifugal compressor consists of blades on a rotating wheel. The compressor wheel is either cast or machined out of one block of aluminum, making it one solid component. By spinning this wheel suction is created in the center and gas or air is forced outward in the radial direction to an outlet point called the compressor discharge. This compressor has many advantages: high pressure ratio, simple design with few moving parts, and a wide operating range between surge and choke limits. They are energy efficient and can move a large volume of gas. Staging these compressors requires a complex piping network, due to the axial inlet and radial outlet directions of gas flow. Compressors of this type are also often seen on turbochargers, where they are powered by a turbine to deliver increased airflow to an internal combustion engine, without the need for ultra high pressures (Bathie, 1996). Since this compressor can provide high flow rates they are sometimes used to compress and transmit natural gas.

The last type of compressor to be discussed is the most useful in the collection, transmission and distribution of natural gas, the reciprocating compressor. In this compressor a piston or series of pistons compress and pressurize the gas. A reciprocating gas compressor has some similarities to a reciprocating engine. They both are piston-cylinder devices connected to a crankshaft. In an engine, fuel is supplied and ignited to produce power though the crankshaft. Conversely, a compressor is supplied power though the crankshaft and the motion of the pistons up and down compress a gas instead of facilitating power production. High pressure ratios can be achieved with this type of compressor, but very high rotational speeds are needed to achieve large volumes of flow. These types of compressors are usually coupled to the driving force by a rotating power shaft. If the engine and compressor share a common crankshaft the unit is called an integral compressor. An integral compressor transfers power directly through the crankshaft and the unit has no external output power shaft. The compressor and engine are built as one unit and are inseparable. The compressor being studied in this experiment is of this type. It is a GasJack Model FI manufactured by Compressco Inc. of Oklahoma City, OK. The GasJack is a V-8 engine where four of the cylinders have been converted from power cylinders to compression cylinders.

In summary of the above literature three main concepts have been found. First NO_x is known to be a function of temperature and time, and CO is known to be a strong function of equivalence ratio (Heywood, 1988). This can be seen in Figure 2.3 in terms of excess air. Second it has been found that NSCR is capable of effectively reducing NO_x and CO under the correct operating conditions. Defoort et al. (2004) found that 95% reduction is possible at an equivalence ratio of 1.014. Lambert (1995) claims that 98% reduction of NO_x and CO is possible with pre-catalyst O_2 levels of 0.5% or less. The final concept from the literature is that the AFRC and O_2 sensor are the key components to a successful NSCR application. Reductions of 90% and above are only possible when the engine is operating at precisely the correct condition. Drift of the AFRC and instability of the O_2 sensor can cause the emission reduction to decline greatly. In the testing of the Compressco GasJack and Emit NSCR system, the ability of the AFRC to maintain control of the engine was studied closely.

CHAPTER 3 - Mathematical Discussion

After reviewing the literature on engine testing and NSCR technology, several parameters which pertain to quantifying the engine's emissions and performance are necessary to calculate. These parameters are fuel flow rate, equivalence ratio, brake power, BSFC, and emission concentrations. Since this project is experimental, the governing equations for the experiment are equations which can be used in data analysis. The main goal of this chapter is to move from the collection of raw data consisting of temperatures and pressures to a fully characterized engine. The first section of this chapter describes how Bernoulli's Equation can be used to calculate flow, the next section takes a look at the first law of thermodynamics and real gas mixtures, the third section describes other standard engine performance parameters. The fourth section describes the approach taken to reduce emissions data to mass based units, and the final section describes in detail the uncertainty analysis used in the project.

Calculating Flow – Bernoulli's Equation

Two flows were calculated on the GasJack for this experiment. On the engine side, fuel mass flow rate was determined and on the compressor side, inlet mass flow rate was calculated. For the fuel flow on the engine side as well as the gas flow on the compressor side a variation on Bernoulli's equation was used. Equation (3.1) shows Bernoulli's equations (White, 2003).

$$\Delta p = p_1 - p_2 = \frac{\rho V_2^{\,2}}{2} - \frac{\rho V_1^{\,2}}{2} + \rho g Z_2 - \rho g Z_1 \tag{3.1}$$

By assuming there is no significant change in potential energy, the last two terms can be dropped and assuming that density is constant it can be factored out which reduces equation (3.1) to equation (3.2).

$$\Delta p = \frac{1}{2}\rho(V_2^{\,2} - V_1^{\,2}) \tag{3.2}$$

Equation (3.3) shows that mass flow rate is equal to density multiplied by cross sectional area and velocity. Figure 3.1 which shows a pipe with an orifice, which is just a reduction in area, where the upstream pipe is section 1, and the orifice is section 2.

$$\dot{m} = \rho A V \tag{3.3}$$

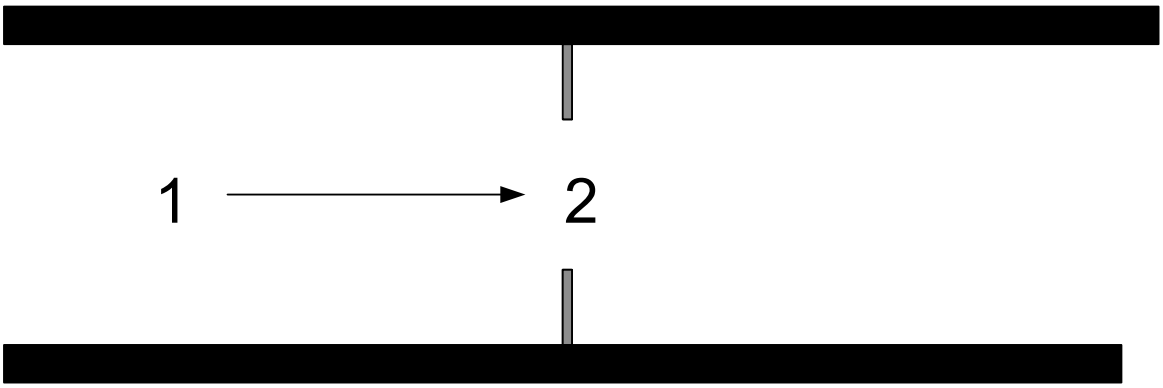

Figure 3.1 Orifice in a Pipe

By solving equation (3.3) for V in terms of A, $\dot{m}$, and ρ and combining with equation (3.2), equation (3.4) is obtained which gives mass flow rate as a function of the pressure drop, the density and the flow areas.

$$\dot{m} = \frac{A_2\sqrt{2\Delta P\rho}}{\sqrt{1-\left(\frac{A_2}{A_1}\right)^2}} \tag{3.4}$$

By defining beta as the ratio of the diameters in 1 and 2, equation (3.4) can be finally reduced to equation (3.5).

$$\dot{m} = \frac{\frac{\pi}{4}d_2^{\,2}\sqrt{2\Delta P\rho}}{\sqrt{1-\beta^4}} \tag{3.5}$$

The theoretical mass flow rate through an orifice is given by equation (3.5). However, through much experimental data it is known that the theoretical flow rate does not match experimental flow rates. Therefore, a coefficient of discharge is introduced to improve the accuracy of this equation. The coefficient is determined experimentally and provided by the manufacturer with a specific orifice. A further improvement of the flow rate can be made by adding a coefficient for gas expansion, which can be calculated by (Cusick, 1961):

$$Y = 1-(0.41+0.35\beta^4)\frac{\Delta p}{p(-0.0003T+1.3263)} \tag{3.6}$$

Finally the actual mass flow rate is given by:

$$\dot{m} = C_D Y\frac{\frac{\pi}{4}d_2^{\,2}\sqrt{2\Delta p\rho}}{\sqrt{1-\beta^4}} \tag{3.7}$$

Calculating Power – Energy Balance

To calculate the power the engine is delivering to the compressor, an energy balance was performed on the compressor. This is corollary to the brake power measured by a dynamometer. By measuring pressure and temperature on both the inlet and discharge sides of the compressor, the change in enthalpy was calculated. The enthalpy was calculated based on a sum over all gas components of the ideal molar gas cubic polynomial plus the isothermal departure from the ideal case. This is expressed as equation (3.8) (Francis).

$$h = \sum_{i=1}^{n} x_i h_i + R_c \Delta h_t \tag{3.8}$$

The first term is the sum of each enthalpy over the all gas components. It expands to equation (3.10). By using the actual gas composition, this gives a very good representation of the actual enthalpy at a given temperature.

$$h_i = A_i + B_i T + C_i T^2 + D_i T^3 \tag{3.9}$$

$$\begin{aligned}\sum_{i=1}^{n} x_i h_i = {} & x_1\left(A_1 + B_1 T + C_1 T^2 + D_1 T^3\right) + x_2\left(A_2 + B_2 T + C_2 T^2 + D_2 T^3\right) + \ldots \\ & + x_n\left(A_n + B_n T + C_n T^2 + D_n T^3\right)\end{aligned} \tag{3.10}$$

To incorporate real gas behavior into the enthalpy calculation, the second term in equation (3.8) is calculated by (Francis):

$$\Delta h_t = \left(B_o RT - 2A_o - \frac{4C_o}{T^2}\right)\rho + \frac{\rho^2}{2}\left(2bRT - 3a\right) + \frac{6\rho^5 a\alpha}{5} + \frac{c\rho^2}{T^2}\left(\frac{3}{\gamma\rho^2} + \left(\gamma\rho^2 - \frac{3}{\gamma\rho^2} - \frac{1}{2}\right)e^{-\gamma\rho^2}\right) \tag{3.11}$$

The Δh_t term uses eight empirical constants, A_o, B_o, C_o, a, b, c, α, and γ as well as ρ the density. The 8 empirical constants are calculated according the ideal gas mixture rules and are shown in equations (3.12) to (3.19). Density is obtained by solving the Benedict-Webb-Rubin (BWR) equation by Newton's method. Equation (3.20) shows the BWR equation.

$$A_o = \left(\sum_{i=1}^{n} x_i A_{oi}^{\,1/2}\right)^2 \tag{3.12}$$

$$B_o = \frac{1}{8}\sum_{i=1}^{n}\sum_{j=1}^{n} x_i x_j \left(B_{oi}^{\,1/3} + B_{oj}^{\,1/3}\right)^3 \tag{3.13}$$

$$C_o = \left(\sum_{i=1}^{n} x_i C_{oi}^{\,1/2}\right)^2 \tag{3.14}$$

$$a = \left(\sum_{i=1}^{n} x_i a_i^{1/3}\right)^3 \tag{3.15}$$

$$b = \left(\sum_{i=1}^{n} x_i b_i^{1/3}\right)^3 \tag{3.16}$$

$$c = \left(\sum_{i=1}^{n} x_i c_i^{1/3} \right)^3 \tag{3.17}$$

$$\alpha = \left(\sum_{i=1}^{n} x_i \alpha_i^{1/3} \right)^3 \tag{3.18}$$

$$\gamma = \left(\sum_{i=1}^{n} x_i \gamma_i^{1/2} \right)^2 \tag{3.19}$$

$$P = \rho RT + \left(B_o RT - A_o - \frac{C_o}{T} \right) \rho^2 + \left(bRT - a \right) \rho^3 + a\alpha\rho^6 + \frac{c\rho^3}{T^2} \left(1 + \gamma\rho^2 \right) e^{-\gamma\rho^2} \tag{3.20}$$

To make the calculation for horsepower, a program called "AGA MARK 2" was used. This is a program developed by the compression energy task group engineering and operations analysis committee of the American Gas Association (AGA) (Francis). The program was used to determine the enthalpy at suction and discharge conditions in the compressor. After calculating the enthalpy, a first law energy balance is used to find the power, assuming negligible heat transfer and changes in kinetic and potential energy. This is given by equation (3.21).

$$\dot{W}_b = \dot{m} \left(h_D - h_S \right) \tag{3.21}$$

Calculating Other Engine Performance Parameters

Since air flow is not directly measured, the equivalence ratio is calculated based on an exhaust gas relation given by Ferguson and Kirkpatrick (2001). By writing the combustion reaction as shown in equation (3.22), the equivalence ratio can be determined from exhaust gas composition. Equation (3.23) shows how equivalence ratio was determined, this expression can be obtained by applying a carbon and oxygen balance on the combustion reaction. By calculating the equivalence ratio in this method, the results would be within two percent of a directly measured equivalence ratio. The exhaust gas was dried prior to measurement by the analyzer and therefore equation (3.24) was used to determine the dry mole fraction of water (Ferguson and Kirkpatrick, 2001).

$$C_\alpha H_\beta O_\gamma N_\delta + \frac{a_s}{\phi} \left(O_2 + 3.76 N_2 \right) \rightarrow n_1 CO_2 + n_2 H_2 O + n_3 N_2 + n_4 O_2 + n_5 CO + n_6 H_2 + n_7 CH_z \tag{3.22}$$

$$\phi = \frac{2 \left(1 + \frac{1}{4} \frac{\beta}{\alpha} - \frac{1}{2} \frac{\gamma}{\alpha} \right) \left(y_1^o + y_5^o + y_7^o \right)}{2 y_1^0 + y_2^o + 2 y_4^o + y_5^o} \tag{3.23}$$

$$y_2^o = \frac{\frac{1}{2} \frac{\beta}{\alpha} \left(y_1^o + y_5^o \right)}{1 + \frac{y_5^o}{3.5 y_1^o}} \tag{3.24}$$

As seen in the combustion reaction, the general fuel is made up of carbon, hydrogen, oxygen and nitrogen. The actual natural gas composition was reported by the gas company and was used in all calculations. The natural gas composition used was:

$$C_{1.010}H_{3.877}O_{0.047}N_{0.049} \tag{3.25}$$

The brake specific fuel consumption is then calculated from the fuel mass flow rate and power. In natural gas fueled engines, it is customary to multiply the general equation for BSFC by the lower heating value to obtain units of BTU/hp-hr. This is given in equation (3.26).

$$BSFC = \frac{\dot{m}_{fuel}}{\dot{W}_b} LHV \tag{3.26}$$

Thermal efficiency is how effective an engine is at transferring chemical potential energy contained in a fuel to useful mechanical energy. It is calculated using the brake power, fuel flow rate and the lower heating value of the fuel:

$$\eta_{th} = \frac{\dot{W}_b}{\dot{m}_{fuel} LHV_{fuel}} \tag{3.27}$$

Calculating Mass Based Emissions

When measuring emissions, gas analyzers take readings in parts per million volume, or ppmv. Parts per million is a unit of concentration. Regulated quantities are typically given on a mass basis instead of concentration, therefore ppmv emissions must be converted to g/hp-hr. To make the conversion consistent, the EPA recommends using method 19 to determine exhaust gas flow rate (Ely, 2004). EPA Method 19 based on the O_2 F-factor was used in the data analysis for this experiment. Equation (3.28) shows how the exhaust flow rate is found.

$$Q = HHV \times 10^{-6} \dot{m}_f F_{O_2} \left(\frac{20.9\%}{20.9\% - O_2\%_{measured}} \right) \tag{3.28}$$

The parameter *HHV* is the higher heating value of the fuel used, $\dot{m}_f$ is the fuel flow rate and F_{O_2} is a defined value given by the EPA. After calculating the flow rate of the exhaust, Q, the density of each exhaust gas component must be determined. Table 3.1 was used to find the density factors for the most commonly measured exhaust gas components.

Table 3.1 Density Factors for Exhaust Gases

Source: Ely, 2004

Component	Density Factor (ρ)
NO_x	1.194×10^{-7} lb_m/ft^3-ppmv
CO	7.26×10^{-8} lb_m/ft^3-ppmv
Oxygen	4.155×10^{-8} lb_m/ft^3-ppmv
NO	7.792×10^{-8} lb_m/ft^3-ppmv

After calculating the exhaust gas flow rate and choosing the density which corresponds to the species being used, equation (3.29) can be used to calculate the brake specific mass based emission rate of exhaust (Ely, 2004). Where E_{ppmv} is the concentration given by the gas analyzer, ρ is the density of the component being calculated, Q is the exhaust gas flow rate, and $\dot{W}_b$ is the brake power the engine was operating at when the sample was taken.

$$E_{mass} = \frac{E_{ppmv}\rho Q}{\dot{W}_b} \tag{3.29}$$

Mass based emissions were calculated for pre- and post-catalyst exhaust gas at each operating point. Therefore to determine the percent reduction in emissions or catalyst efficiency, either the ppmv values or the mass specific values can be used. Equation (3.30) shows the catalyst efficiency based on mass specific values.

$$\eta_{catalyst} = \frac{E_{mass\ pre-catalyst} - E_{mass\ post-catalyst}}{E_{mass\ pre-catalyst}} \tag{3.30}$$

Uncertainty Analysis and Propagation of Error

In any experimental project, the results and conclusions are only as good as the exactness to which the data is known. This experiment is no exception, therefore each measurement was made by a calibrated instrument, and when data was collected, each point was measured numerous times to reduce any data inconsistencies. However, even while striving for the highest accuracy of measurements, some uncertainty is always introduced along with experimental measurements. To account for the uncertainty, the standard deviation of a data set was calculated and used as the uncertainty from a measurement. When the mean value of each measurement is passed through series calculations, the standard deviation or uncertainty is passed along as well. The approach that was used in propagating the uncertainty through the

calculations is described by Bevington and Robinson (2003). The following equations were used (Bevington and Robinson, 2003). In the equations below, X is used as the calculated variable, Y and Z are the measured values with some uncertainty σ_y and σ_z, which yield some uncertainty σ_x, while a and b are constants. Equation (3.31) shows the uncertainty from additions or subtraction.

$$X = aY \pm bZ$$
$$\sigma_x = \sqrt{a^2 \sigma_y{}^2 + b^2 \sigma_z{}^2} \tag{3.31}$$

Equation (3.32) shows the uncertainty from multiplication or division.

$$X = aY \cdot bZ$$
$$\sigma_x = X\sqrt{\frac{\sigma_y}{Y} + \frac{\sigma_z}{Z}} \tag{3.32}$$

Equation (3.33) shows the uncertainty from raising a variable to a constant power.

$$X = aY^b$$
$$\sigma_x = bX\frac{\sigma_y}{Y} \tag{3.33}$$

These are the equations needed to propagate the uncertainty through the calculations performed for this experiment.

For an example of how to propagate uncertainty through a series of calculations, recall equation (3.7):

$$\dot{m} = C_D Y \frac{\frac{\pi}{4} d_2{}^2 \sqrt{2\Delta p \rho}}{\sqrt{1-\beta^4}}$$

To calculate mass flow rate, the parameters, Y, ΔP, and ρ are used. The following example shows how the uncertainty would be determined:

Example: Calculation of Uncertainty for mass flow of a compressed gas, equation (3.7)

Variables with known uncertainties

$Y = 0.910 \pm 0.02$

$\Delta p = 60.01 \pm 0.99 \,\text{in}\,\text{H}_2\text{O}$

$\rho = 0.073 \pm 0.001 \dfrac{\text{lb}}{\text{ft}^3}$

Constants with no associated uncertainty

$C_d = 0.6052$

$d = 1.1 \text{in}$

$\beta = 0.6832$

Calculation for the mean value

$$\dot{m} = 0.6052 \times 0.910 \times \frac{\frac{\pi}{4} 1.1^2 \sqrt{2 \times 60.01 \text{in}\,\text{H}_2\text{O} \times \frac{\text{lb}_\text{f}/\text{in}^2}{27.7 \text{in}\,\text{H}_2\text{O}} \times 0.073 \frac{\text{lb}}{\text{ft}^3} \times \frac{\text{ft}^2}{144 \text{in}^2} \times 32.2 \frac{\text{lbft}}{\text{lb}_\text{f}\text{s}^2} \times \frac{3600 \text{s}^2}{\text{min}^2}}}{\sqrt{1 - 0.6832^4}}$$

$\dot{m} = 9.443 \dfrac{\text{lb}}{\text{min}}$

Calculation for the uncertainty

$$\sigma_{\dot{m}} = \dot{m} \sqrt{\left(\frac{\sigma_Y}{Y}\right)^2 + \left(\frac{\sigma_{\Delta P}}{\Delta P}\right)^2 + \left(\frac{\sigma_\rho}{\rho}\right)^2}$$

$$\sigma_{\dot{m}} = 9.443 \frac{\text{lb}}{\text{min}} \times \sqrt{\left(\frac{0.02}{0.910}\right)^2 + \left(\frac{0.99}{60.01}\right)^2 + \left(\frac{0.001}{0.073}\right)^2}$$

$\sigma_{\dot{m}} = 0.289 \dfrac{\text{lb}}{\text{min}}$

End Result

$\dot{m} = 9.443 \pm 0.289 \dfrac{\text{lb}}{\text{min}}$

CHAPTER 4 - Experimental Setup

This chapter details how the experiment was setup at the NGML. To apply the governing equations presented in Chapter 3, correct measurements must be taken. To achieve this, many instruments were installed on the Compressco and this chapter details the purpose and functionality of each. The first sections describe the equipment installed and tested at the lab. The next section details the test cell design, followed by a description of the data collection system and instrumentation used on the GasJack. Finally in the last section the control system is discussed.

GasJack Compressor

Compressco Inc. has been in the compressor business since it began as a field service company in 1990. They began manufacturing their own compressor units and now have 2,595 units in use worldwide. Their compressor is designed for gas collection from marginal wells where there is a need for an economical small compressor. Industry demographics say that 64% of all domestic wells are classified as marginal, but these wells represent only 10% of domestic production. This facilitates a large and ever increasing need for improved technology to utilize these marginal wells. The GasJack compressor is manufactured from a modified rich burn Ford 460 cubic inch V-8 engine. Four cylinders on one side are left in the OEM conditions and used for power while four cylinders on the opposite side are converted into a reciprocating compressor. Power is transferred from the engine side to the compressor side directly through the crankshaft in the engine block (Compressco Inc., 2007). The conversion from the Ford V-8 engine to the Compressco GasJack was completed by a few simple processes. A new compressor head which removed engine valves and other unnecessary components was manufactured to be compatible with the 460 block. The original pistons on the compressor side were replaced with pistons more suitable for compression. The compressor uses two way plate valves to regulate gas pressure and flow, and a new valve cover for the compressor side was designed including intake and discharge flanges for the natural gas.

The GasJack compressor is unique due to the fact that the crankcase is pressurized with natural gas to keep the environment oxygen free. This is done as a safety feature since these

engines run unattended. When natural gas is compressed in a reciprocating compressor there is a possibility for it to leak past the compressor rings and mix with the air in the crankcase, creating a combustible fuel air mixture. To eliminate this possibility in the GasJack, pressurized gas displaces all the air from the crankcase. This eliminates the possibility of a fuel air mixture leaking into and igniting in the crankcase. The crankcase is vented into the carburetor below the throttle plate adding fuel to the already mixed air and fuel charge. Figure 4.1 shows the fuel system on the Compressco GasJack.

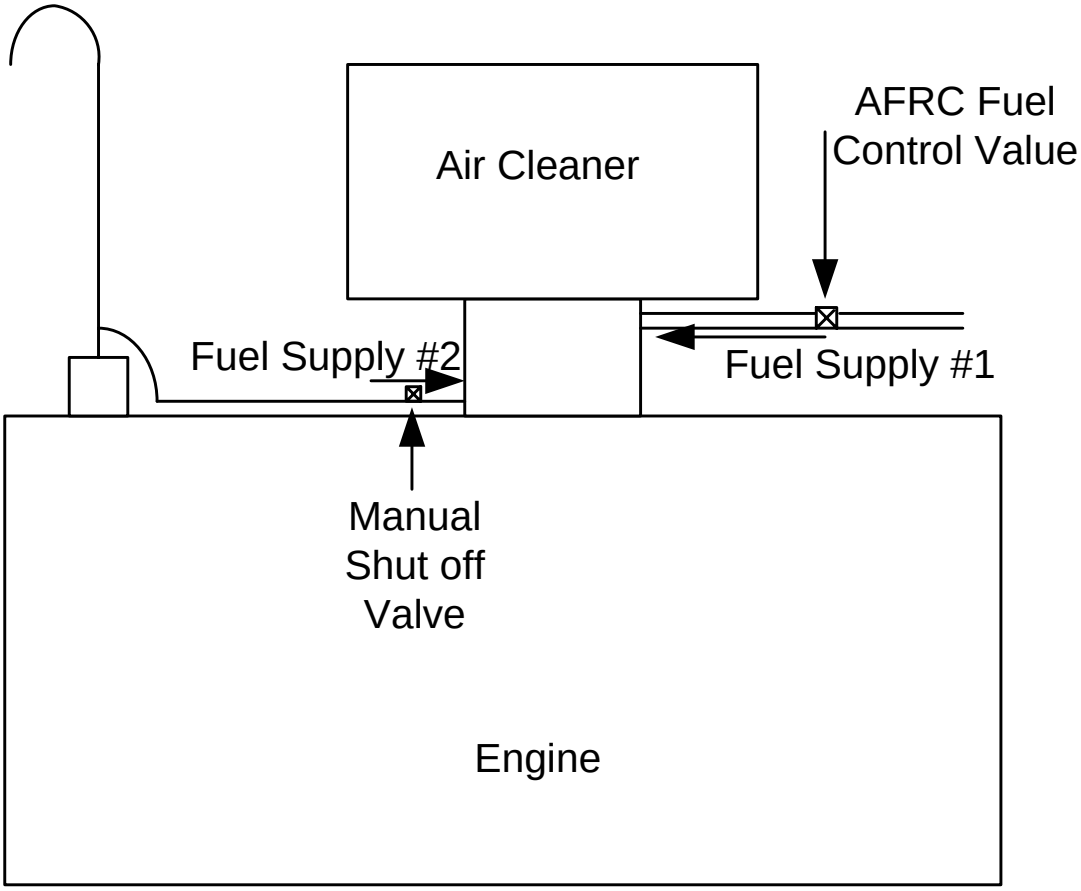

Figure 4.1 GasJack Fuel System

One major advantage of this engine compressor is that the size is compact and all necessary components are included and skid mounted for easy installation. The majority of the unit is made up of Ford 460 engine components making the GasJack a reliable compressor. Additionally, since the compressor is directly connected to the engine by the crankshaft, many losses are avoided such as twisting of the output shaft, changes in mechanical energy through gearing, and losses through additional bearings and seals. This helps improve the efficiency of the GasJack compressor. The simple design of the compressor also allows anyone with basic

automotive knowledge to service and repair the unit. Many of the parts on the GasJack are common with the Ford 460, making parts readily available at local automotive stores. On the contrary, other compressors are very complex in design and parts are available only through the manufacturer. This can require specialized tools, skills and parts making them expensive to maintain and operate (Compressco Inc., 2007). Because of the many advantages of this compressor, market share continues to increase, further facilitating the need for a well understood emissions solution.

The specifications for the test unit from Compressco are as follows. The engine has a bore or 4.36 inches and stroke of 3.85 inches. The speed operating range is from 1,100 to 2,000 rpm. The maximum discharge pressure is 90 psig for the compressor and the displacement is 215 inches (Compressco Inc., 2007). On the model used in the lab for testing, existing safety systems were left in place and augmented with computerized controls and safety. Up until recently, emissions requirements were not regulated for small engines such as a Compressco GasJack and therefore no OEM exhaust gas after treatment comes installed on the unit.

Emit AFRC and NSCR systems

The air-to-fuel ratio controller used for testing was an Emit Technologies Edge NG. The Edge NG controller is specifically designed for rich burn, carbureted, natural gas engines. This AFRC controls the oxygen level in the exhaust gas stream based on readings from an oxygen gas sensor installed in the exhaust piping between the exhaust manifold and the catalytic converter. The controller monitors oxygen levels as well as the temperature rise across the catalyst element. The Edge NG controller also has the capability to alarm and shut down the engine if the oxygen content or exhaust gas temperatures fall out of safe levels (Emit Technologies, 2007).

Emit Technologies has also provided a catalytic converter for testing along with their Edge NG air-to-fuel ratio controller. The model of catalyst being tested is the EAS-1000T. Emit recommends that oxygen levels entering the catalytic converter be in the range of 0.25-0.50% for optimal performance. Additionally they say that pre-catalyst levels of NO_x in the range of 1,000-2,750 ppmv will be reduced to a range of 100-250 ppmv, and a CO range of 3,000-5,500 ppmv will be lessened to 450-1,200 ppmv (Emit Technologies, 2003). While levels can vary from engine to engine, during the testing the pre- and post-converted concentrations was measured and compared with the manufacturer's levels.

Test Cell Design

To fully test the GasJack compressor and Emit systems a test cell was designed and built at the National Gas Machinery Laboratory. The design consisted of a location to install the unit, the addition of infrastructure such as a gas pipe line, electrical wiring, conduit, and a computerized control and data collection system. The compressor is skid mounted with a 4 foot by 12 foot size. The size of a suitable location was determined to be 8 foot by 20 foot to give ample room to work on and around the unit. The skid was setup on a gravel base, similar to a field installation, in the engine test center at the NGML. By choosing this outside location, other infrastructure necessities were simply expanded to meet the needs of the new test cell. The natural gas and electrical infrastructure were extended from the small engine test cell to the Compressco test cell. A computer aided drawing is given in Figure 4.2 of the Compressco test cell which has been added to the NGML engine test center.

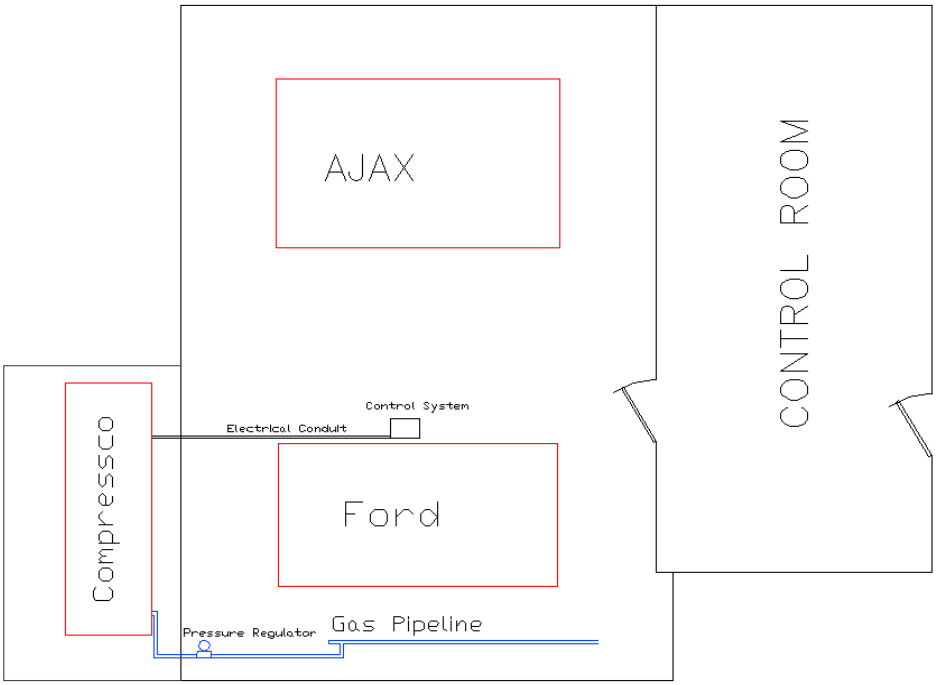

Figure 4.2 NGML Engine Test Center

One major difference between this experiment and most engine tests is that in most engine tests, the engine can be coupled to a dynamometer. This is not a possibility for the Compressco because of the integral compressor. To overcome this limitation, the compressor

was instead used to load the engine. This loaded the engine in a way that most correctly simulates an actual operating condition. In actual operation the engine is used to drive the compressor, so in the lab test, the same was done. However, in the lab setting, there is no place for the pressurized gas to flow, so it was cooled by passing through a radiator and then throttled back to the inlet pressure by a load valve, this can be seen in Figure 4.3.

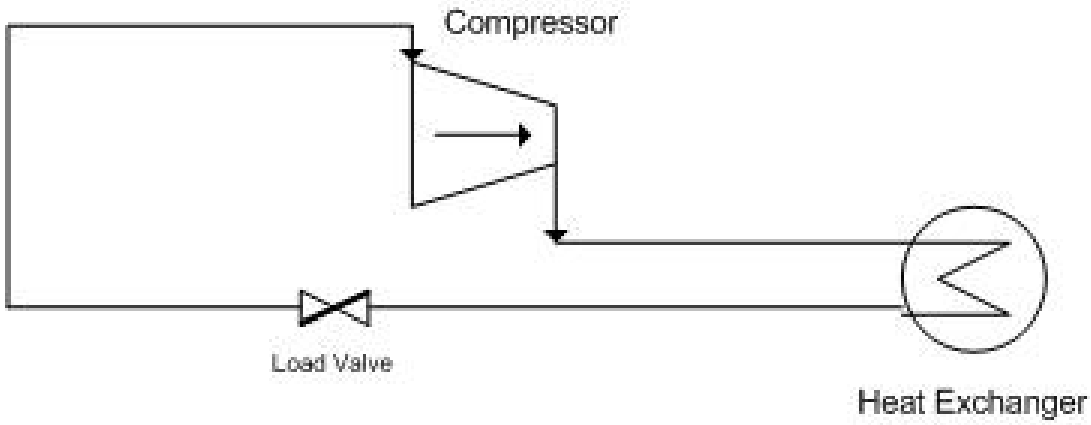

Figure 4.3 Schematic of the Compressor and Engine Loading System

By varying the amount the load valve is opened or closed, the discharge pressure on the compressor can be changed. When the load valve is wide open the compressor, and consequently the engine, was unloaded. Then by closing the valve, the load on the engine can be increased. By monitoring the compressor inlet and discharge gas conditions, an energy balance can be performed to determine the amount of power being used by the compressor. This recycle loop of the compressed gas was beneficial in that it provides a way to load the engine and a way to recycle the compressed natural gas.

Data Collection and Instrumentation

In the previous chapter, several engine performance parameters are discussed as being relevant to engine research. Many of these parameters apply to the research conducted on this engine. The parameters which are quantified are the emissions created by the combustion process, especially NO_x and CO. Additionally, the speed (rpm), brake power (hp) and brake specific fuel consumption (BSFC) were determined to relate the emissions to engine performance. To determine these engine parameters, measurements were made on the engine and compressor which allow engine performance and brake specific emissions to be calculated. The detailed equations and steps to calculate the parameters are given in the mathematical

discussion in Chapter 3. However, to make the calculations, the correct measurements must be made. Table 4.1 gives a list of the instrumentation installed on the engine and compressor, the reason for installing that instrument, and the instrument's uncertainty.

Table 4.1 Instrumentation List

Measurement	To Calculate	Instrument	Uncertainty
Ambient Pressure	Correct data to standard conditions	Omega PX215	0.25%
Ambient Temperature		Kele HO30K-TT-2	1.0%
Ambient Humidity		Kele HO30K-TT2	3.0%
Engine Fuel Flow Differential Pressure	Engine Fuel Mass Flow Rate, BSFC, Thermal Efficiency, Equivalence Ratio	Omega PX771a	0.1%
Engine Fuel Pressure		Omega PX725	0.1%
Engine Fuel Temperature		Type K Thermocouple	3.96°F
Compressor Flow Differential Pressure	Compressor Mass Flow Rate, Inlet Gas Enthalpy, Power	Omega PX771	0.1%
Compressor Inlet Pressure		Omega PX725	0.1%
Compressor Inlet Temperature		Type K Thermocouple	3.96°F
Compressor Exit Pressure	Compressed Gas Enthalpy, Power	American Sensor Technology AST4700	0.25%
Compressor Exit Temperature		Type K Thermocouple	3.96°F
Engine Speed		Magnetic Pickup	0.5%
O_2	Mass Based Emissions	ECOM J2KN	0.2%
CO	Mass Based Emissions	ECOM J2KN	0.2%
NO	Mass Based Emissions	ECOM J2KN	0.2%
NO_2	Mass Based Emissions	ECOM J2KN	0.2%

Figure 4.4 shows a schematic of the engine and compressor along with all the instrumentation that was added.

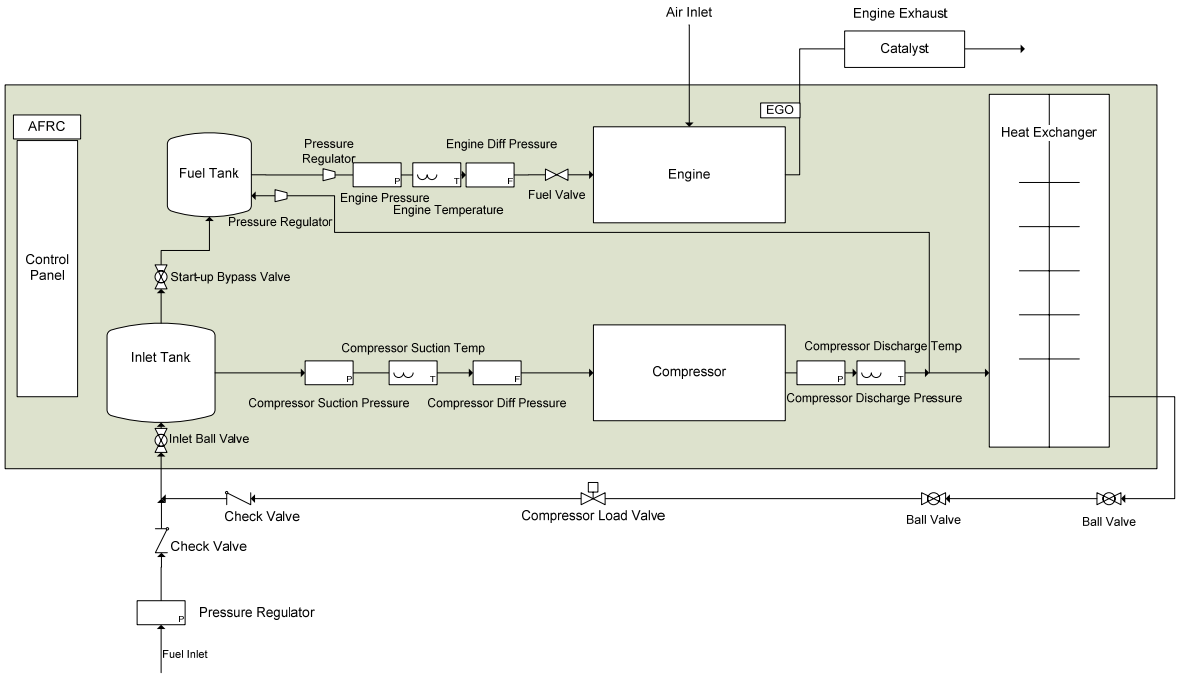

Figure 4.4 Compressco Layout

On the engine side, the calculated parameter needed is the mass flow rate of fuel. To obtain the mass flow rate of fuel, an orifice plate was installed on the fuel inlet line upstream of the carburetor. The pressure drop across the orifice plate was measured with a differential pressure transducer. The pressure and temperature of the gas were also measured before the orifice plate to find density. On the compressor, a similar technique was used to find the mass flow rate on the inlet side of the compressor measuring pressure, temperature, and pressure drop through an orifice plate. To determine the power the compressor uses, the discharge pressure and temperature were also measured. This allowed the enthalpy of the gas to be calculated at both suction and discharge conditions. Then by applying an energy balance to the compressor, power was calculated. The final measurement was the composition of the exhaust gas of the engine. The concentration was measured both before and after the catalyst to determine the efficiency of the catalyst. This was measured using an ECOM portable gas analyzer.

The data from the measurements in Table 4.1 was collected through a program written in OPTO22. OPTO22 is a computer based control system that was used in this project for both

control and data collection. Figure 4.5 shows a screen shot of the graphical user interface that was developed for the test cell. When the record data button is pressed, data was measured and recorded every 1 second for 5 minutes giving a total of 300 data point for each test point. These data points were then collected in a spreadsheet. A spreadsheet program was developed to perform calculations from the data points. When the raw data points are entered into the spreadsheet, the mean and standard deviation of the points are calculated. Due to measuring each point multiple times, the standard deviation is a good measure of the uncertainty. In preliminary testing, it was found that the standard deviation was dominant over the instrument accuracy. Since repeated measurements were taken on all instruments, except ambient conditions, the uncertainty was in effect measured and reported during the test by the standard deviation. Because of this, the standard deviation was used instead of the instrument's given accuracy. Ambient conditions were measured by another control system at the laboratory and were manually entered into the Compressco data collection system. Therefore ambient condition uncertainty was based on the instrument accuracy. The spreadsheet calculates all the engine parameters given in Chapter 3 from the raw data collected on the engine and compressor.

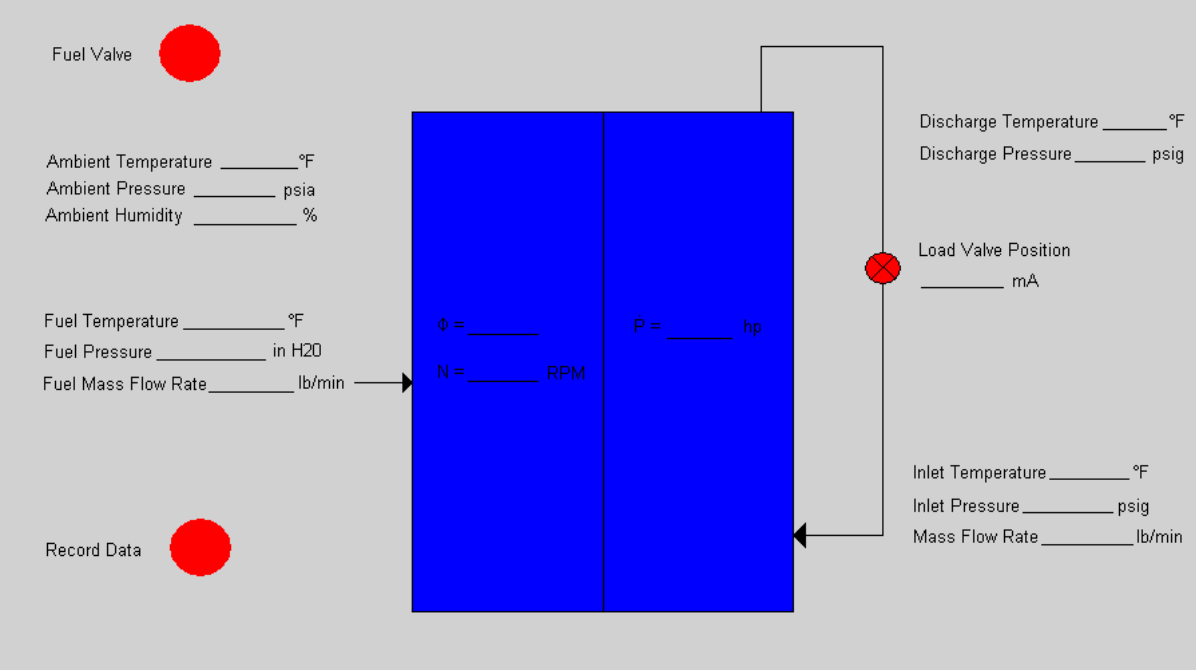

Figure 4.5 Compressco User Interface

Control System

The GasJack contains all the necessary controls on the unit for basic functionality. For simplicity, all OEM controls were left on the skid. However, two additional controls were added through the OTPO22 program. The OPTO22 program was used to control the load valve on the compressor and an automatic gas shut down button was added to the control screen for safety. The rest of the engine control was preformed manually at the GasJack control panel. The control panel is a user interface which allows the engine to be started and stopped. It contains gauges for both the engine and compressor. The engine speed is controlled manually on the engine through the fuel governor. Also on the control panel are Murphy switches that trip and shut the engine down to protect the unit if an over limit situation occurs. Table 4.2 lists the safety systems on the GasJack. If any of these conditions are met, the engine will automatically shutdown to prevent damage.

Table 4.2 Safety Shut Downs

High Discharge Pressure	90 psig
High Suction Pressure	10 psig
Low Suction Pressure	20 inHg
High Discharge Temperature	320°F
Low Engine Oil Pressure	15 psig
High Engine Water Temperature	220°F
High Engine Vacuum	22” Hg
Low Engine Vacuum	2” Hg
Engine Over Speed	2,000 rpm
Excessive Engine Vibration	Not Specific

An operating guide was created from the manufacturer’s operation manual along with some steps specific to this installation. This operating guide can be found in Appendix A.

CHAPTER 5 - Test Results and Discussion

In this chapter the test plan is discussed first, followed by test results and discussion. The test plan consists of the number of test points taken and under what conditions each test was performed. Next there is a description of the uncertainty of the data presented in the results section. At the end of this chapter the emissions test results are given graphically to help visualize trends.

Test Plan

The goal or objective of this project is to characterize the Compressco GasJack engine emissions when operating with an NSCR system. To achieve this, the engine was operated throughout its normal operating range, and tested for brake specific emissions, brake specific fuel consumption, and power. The engine generally operates at 1,800 rpm, has maximum speed of 2,000 rpm, and never is operated below 1,600 rpm. Therefore these three speeds were used to take test data: 1,600, 1,800, and 2,000 rpm. In the field, loading of the engine depends on well pressure and downstream line conditions. To test the engine the compressor suction pressure was held constant at nine psig and compressor discharge pressure was varied to simulate different loading conditions. The maximum discharge pressure for this compressor is 90 psig. To obtain a representative sample of data, information was taken at 100, 90 and 80 percent of the maximum discharge pressure. These values are 90, 81 and 72 psig. These three speed lines and three discharge conditions give a map of the typical operating ranges the compressor would see in field operation. These test points were performed with the AFRC set to auto control mode at the manufacturer's recommended level of 777 mV from the EGO sensor. The test matrix is shown as Table 5.1.

Table 5.1 Test Matrix

		Speed		
		1600 rpm	**1800 rpm**	**2000 rpm**
Discharge Pressure	**72 psig**	Point 1	Point 4	Point 7
	81 psig	Point 2	Point 5	Point 8
	90 psig	Point 3	Point 6	Point 9

Prior to testing each day, the emissions analyzer was calibrated with certified calibration gases to ensure accurate readings. First, the gas analyzer was turned on and allowed to zero all readings, in atmospheric air. Next, the sample line was connected to a bottle of gas, then the analyzer sampled gas for five minutes until the reading stabilized. After the reading was stabilized, if the reading was off, the actual value was entered into the gas analyzer to correct the span. This was preformed for each gas sampled. The calibration gases used were 4,000 ppm CO, 450 ppm CO, 3000 NO, 190 ppm NO, 95 ppm NO_2.

As discussed in Chapter 4, the fuel flow rate is measured to quantify engine performance parameters. The fuel flow rate is measured in the main inlet line to the carburetor. However, fuel is also supplied to the engine through a second smaller line. To quantify the fuel flow rate through the second line the air-to-fuel ratio control system was used. Test points were taken with the supplemental fuel line turned on and off, which allows the secondary fuel flow rate to be calculated. This was done according to the following procedure:

- A test point was recorded at a set air-to-fuel ratio, power and speed with the supplemental fuel valve open;
- The supplemental fuel supply valve was closed, causing the AFRC to detect the leaner mixture and increase the opening of the main fuel supply valve;
- A second test point was recorded at the same air-to-fuel ratio, power and speed as the first;
- Repeat the procedure for all three speeds.

The mass flow rate of the fuel through the main fuel line was increased in the second test by the amount of flow through the supplemental fuel line in the first test. It was found that the supplemental fuel line always supplied the same amount of fuel.

After testing to determine the supplemental fuel flow rate, testing over the engine's operating range for emissions was completed according to the test matrix in Table 5.1. The test procedure was:

- Tune engine into the desired operating point and allow all measured parameters to stabilize;
- Hook up the emissions analyzer to the pre-catalyst test port and watch for trends to become steady;
- Record data every second:

    - Five minutes on the engine
    - Ten minutes on the emissions analyzer
- Move the emissions analyzer to the post-catalyst test port and watch for trends to become steady;
- Record data every one second:
    - Five minutes on the engine
    - Ten minutes on the emissions analyzer

The testing was preformed once and then repeated to ensure accuracy of the results.

Expected Outcomes

In the literature, De Foort et al. (2004), found that NSCR can be effective at 80% or greater reduction of NO_x and CO with the proper control. Since the engine will be operated at steady state, it is expected that the air-to-fuel ratio controller will be able to maintain control and keep the NSCR functioning with reduction of at least 80% for both CO and NO_x. However, due to the steep curve of the EGO sensor, it is expected that some drift of the controller and therefore emission levels will be noticed during testing. It will be determined if the amount of drift by the AFRC will cause the engine's pre- and post-catalyst exhaust gas concentrations to drift significantly as well.

Uncertainty

As discussed in Chapter 3 the uncertainty in any measurement from instrumentation was propagated through to the calculated values. Table 5.2 gives a list of the calculated parameters and uncertainty seen during a typical test point.

Table 5.2 Measured Value Uncertainty

Parameter	Uncertainty (%)
Speed (rpm)	0.2%
Power (hp)	2.8%
Torque (ft-lb_f)	2.8%
BSFC (lb/hp-hr)	5.5%
Fuel Flow Rate (lb/min)	4.5%
Compressor Flow Rate (lb/min)	2.6%
Oxygen Concentration (%)	0.1%
Pre-Catalyst NO_x (g/bhp-hr)	8.6%
Pre-Catalyst CO (g/bhp-hr)	8.9%
Post-Catalyst NO_x (g/bhp-hr)	**27.1%**
Post-Catalyst CO (g/bhp-hr)	**29.0%**

As seen in the table, the highest uncertainties are seen in the post-catalyst emission concentrations. During testing it was found that the values of both CO and NO_x had large fluctuations with time. Because of this the uncertainty is high when measuring post-catalyst emissions.

To understand the high levels of uncertainty in the engine's emissions, the ppm values are plotted against time in the following figures. Figure 5.1 shows the pre-catalyst NO_x emissions from a test point at 1,600 rpm and 72 psig CDP.

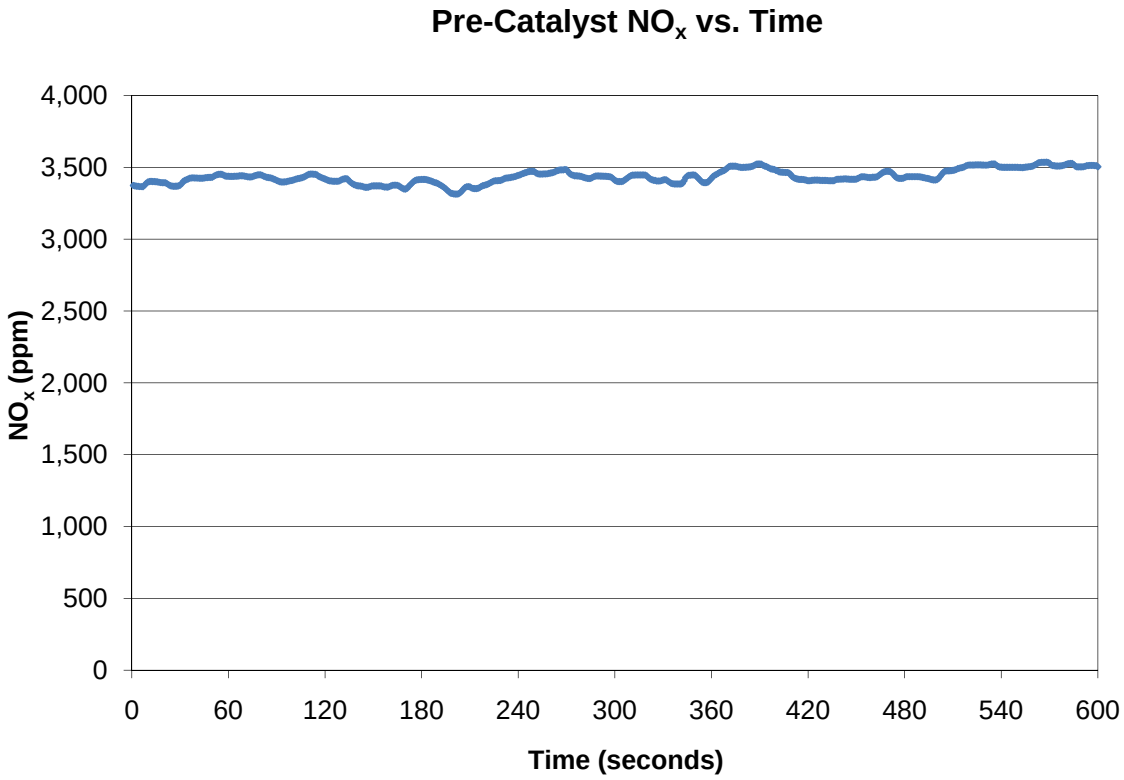

Figure 5.1 Typical Pre-Catalyst NO_x Curve

The mean value over 600 seconds or 10 minutes is 3,335 and has a standard deviation of 37, by dividing the standard deviation by the mean, the coefficient of variation can be calculated to see how much variation there is in the data. The COV in this case works out to be 1%. This is much lower than the 8.6% for pre-catalyst NO_x given in Table 5.2. The NO_x uncertainty is increased when calculating the emissions in grams per horsepower-hour due to combining uncertainty from several measurements. The largest uncertainty comes from the oxygen percentage. At this test point the mean value of the pre-catalyst oxygen level was 0.8% and had and uncertainty of 0.1%. After combining all the uncertainties that go into mass specific emissions a value of 8.6%, on average, is achieved.

Figure 5.2 shows pre-catalyst CO concentration vs. time.

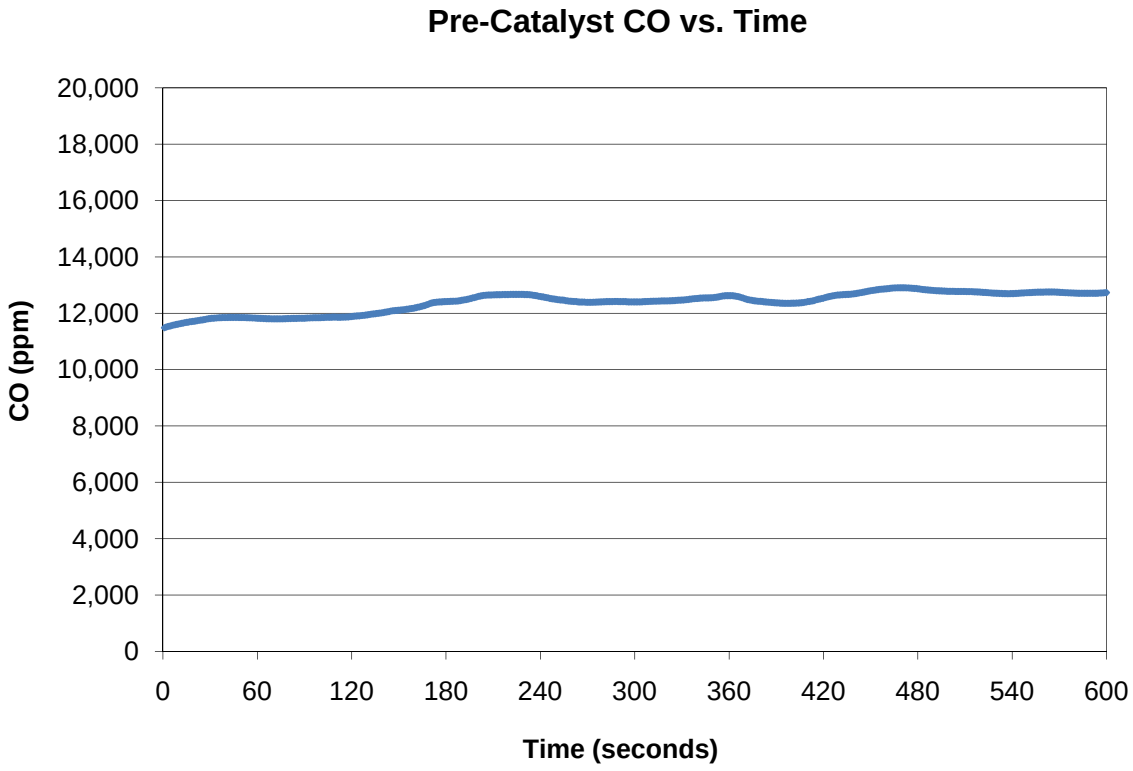

Figure 5.2 Typical Pre-Catalyst CO Curve

The mean value for the CO was 12,392 ppm with a standard deviation of 341. The COV for this test point is 3%, again lower than the 8.9% given in Table 5.2. The reason for the higher uncertainty in the table again occurs for the same reasons as the pre-catalyst NO_x.

Trends versus time for post-catalyst emissions are very different than what was found in pre-catalyst testing. In pre-catalyst testing of emissions, the ppm concentrations of NO_x and CO were stable over time and most of the uncertainty in the brake specific emission values is introduced from the oxygen measurement. This was not the case for the post-catalyst emissions. Figure 5.3 plots post-catalyst NO_x plotted against time.

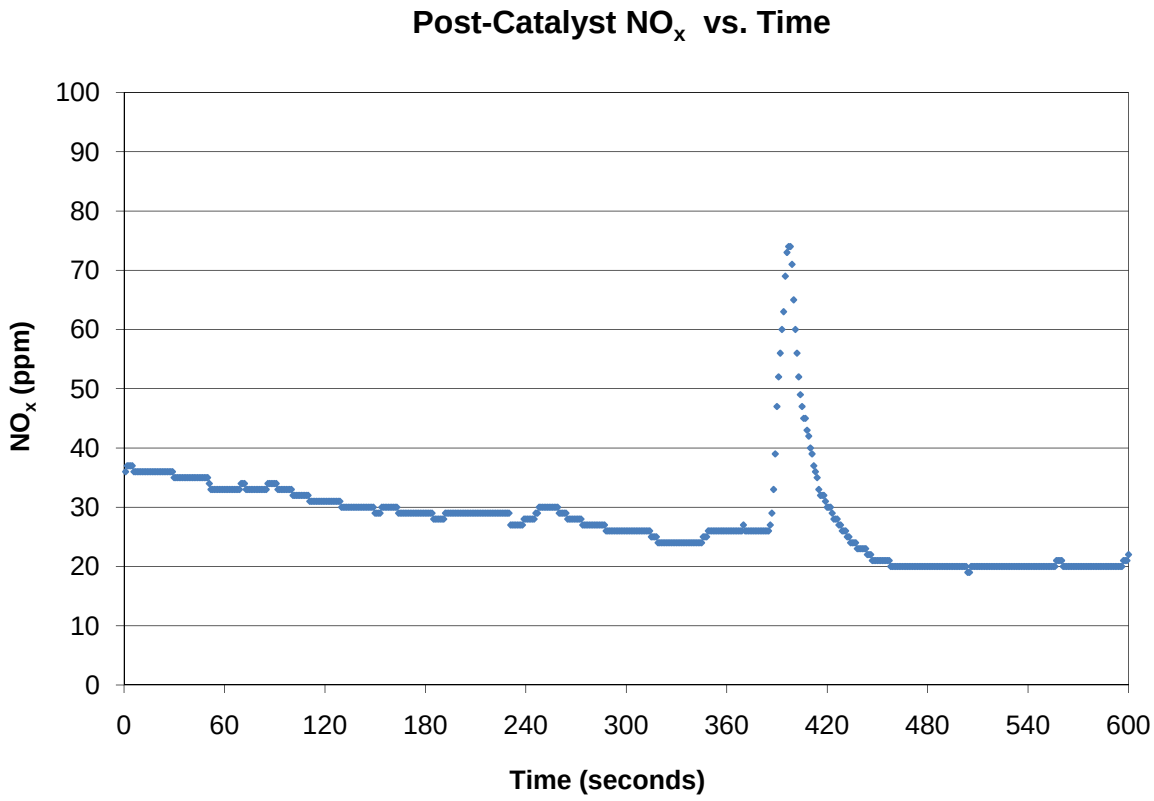

Figure 5.3 Typical Post-Catalyst NO_x Curve

The post-catalyst NO_x displays a slight trend downward followed by a large short spike. The mean and standard deviation of this data set are 28 and 3. The coefficient of variation for this data is 10%. When comparing this COV to the pre-catalyst NO_x COV, which was 1%, this has 10 times more statistical uncertainty. After combining all the uncertainties which make up the mass specific emissions, spikes such as this one or slow drifts upwards or downwards cause the large uncertainty in NO_x.

Figure 5.4 shows post-catalyst CO concentration in ppm vs. time.

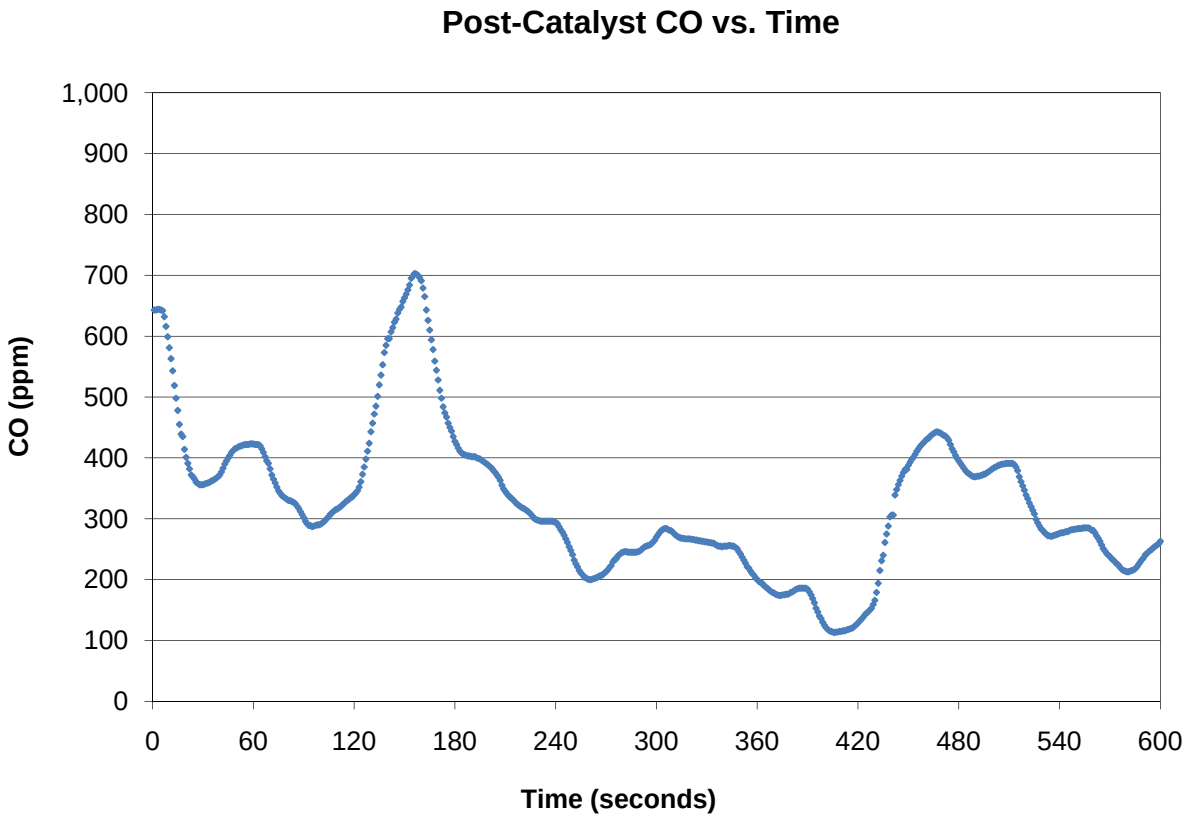

Figure 5.4 Typical Post-Catalyst CO Curve, 3/11/2008

The ppm values of CO vary in time from a peak of 700 ppm to a low of 114 ppm. This high degree of fluctuation is typical of all test results for post-catalyst CO. For this data set the mean is 326 ppm with a standard deviation of 127. This gives a statistical uncertainty of 39% which dominates all other uncertainties as it is propagated into the mass based emissions units. Figure 5.5 shows another graph of post-catalyst CO vs. time.

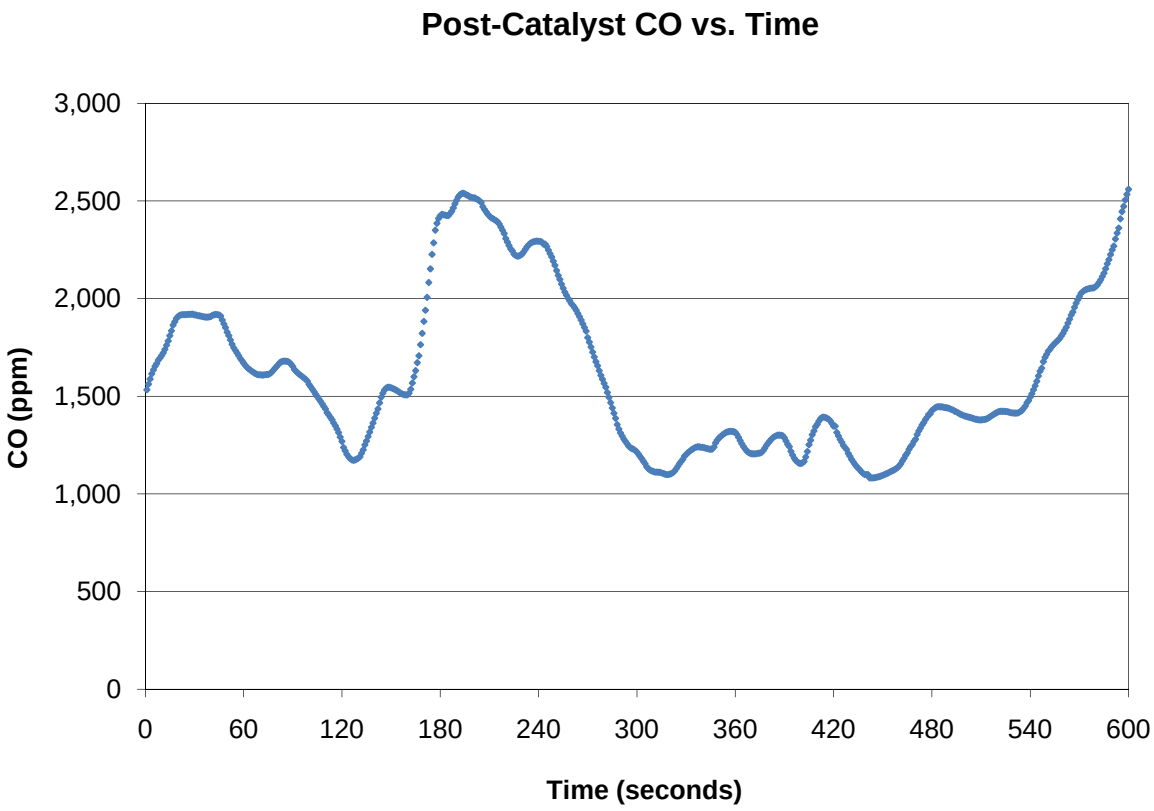

Figure 5.5 Typical Post-Catalyst CO Curve, 3/12/2008

While the mean is clearly higher in Figure 5.5 than Figure 5.4 the statistical uncertainty remains in the same range, 28% vs. 39%. The mean and standard deviation for CO was used when calculating mass based emissions making the uncertainty high. Since the high uncertainty is due to actual variation in the data there is no way to lower the uncertainty. The best way to obtain useful data in the constraints of this experiment was to lengthen the time over which sampling was performed. By taking data for a full 10 minutes, several peaks and valleys were seen indicating that the data was range bound to the high and low of the recorded data. In this sense the mean was a good indicator of what the CO ppm value would average at a constant engine speed and power as it operates over time.

Since CO is a strong function of air-to-fuel ratio, the fluctuation could be due to small changes in the fuel flow rate with a constant air flow rate as the air-to-fuel ratio controller moves the fuel control valve in real time to keep the EGO sensor at the desired set point. To determine whether or not the controller was causing the CO dithering, six additional test points were taken

beyond the points identified in the test matrix. The compressor is typically operated between 1,800 rpm and 2,000 rpm at maximum allowable discharge pressure. Therefore testing was done at:

- Three test points at 1,800 rpm and 90 psig discharge
- Three test points at 2,000 rpm and 90 psig discharge

At these six test points the engine was brought to the desired speed and CDP and allowed to stabilize. Next the AFRC was switched from auto mode to off mode, which disabled any movement of the fuel control valve. A test point was then performed as usual, but additionally a reading of the EGO sensor value was recorded manually before and after each phase of the test. In testing with the AFRC set to auto mode, the output mV reading at the controller was always centered at 777 mV with fluctuations of plus or minus 10 mV. This value, seen on the controller display screen, is heavily averaged internally by the control system before it is seen by the user. Therefore, when the controller is in auto mode, it appears to do an excellent job of keeping the EGO sensor output at the desired set point. When testing with the controller turned off, after 20 minutes the signal often showed minimal drift from the desired set point. Table 5.3 shows the six test points with the controller off and the corresponding EGO sensor output at three different times throughout the duration of one complete test point. The three times a reading was taken were at the beginning of the test when the controller was turned off, after the pre-catalyst emissions test completed, and after the post-catalyst emissions test was completed. The first reading was always at 777 mV because it was taken just as the controller was switched from auto to off mode.

Table 5.3 Test of Air-to-Fuel Ratio Controller

Speed (rpm)	CDP (psig)	Time	Actual mV	Valve Position
		start of test	777 +/-10	133
1793.2	89.9	end of pre-catalyst test	757 +/-10	133
		end of post-catalyst test	738 +/-10	133
		start of test	777 +/-10	115
1802.7	89.6	end of pre-catalyst test	782 +/-10	115
		end of post-catalyst test	767 +/-10	115
		start of test	777 +/-10	116
1796.8	89.8	end of pre-catalyst test	777 +/-10	116
		end of post-catalyst test	787 +/-10	116
		start of test	777 +/-10	214
1997.5	89.6	end of pre-catalyst test	777 +/-10	214
		end of post-catalyst test	787 +/-10	214
		start of test	777 +/-10	186
1993.7	89.1	end of pre-catalyst test	777 +/-10	186
		end of post-catalyst test	767 +/-10	186
		start of test	777 +/-10	208
2004.2	89.6	end of pre-catalyst test	777 +/-10	208
		end of post-catalyst test	777 +/-10	208

As seen in Table 5.3 at the start of each test the EGO sensor indicated a reading of 777 mV. This again proves that the AFRC does keep the sensor output at the desired set point with fuel valve control. However, for three identical test points the valve position to obtain 777 mV at the start of a test had significant variation. The most pronounced example of this is the difference in the fourth and fifth tests which were valve positions of 186 and 214 at the 2,000 rpm and 90 psig tests. The fuel control valve has a maximum opening of 250, so a difference of 28 is 11% of the full scale. With the precision needed for optimal performance of the catalyst, the EGO sensor did not always give consistent enough output values to achieve a specific air-to-fuel ratio. Keeping the valve at a constant position over the entire test did not cause a significant amount of drift of the EGO sensor output in five of the six tests. Only in the first test did the EGO mV reading decline throughout the test. When examining the graphs of CO versus time, similar trends were found as those where the AFRC controller was in auto mode. Since the EGO sensor

set point did not move a significant amount in most tests and the post-catalyst CO showed fluctuations similar to previous results, it was determined that the AFRC is not causing the dithering of post-catalyst CO concentrations.

The fluctuations seen in the post-catalyst CO versus time can be attributed to natural dithering in the catalyst. The dithering in the catalyst occurs due to the storage and release of oxygen into the metallic honeycomb structure. As oxygen is absorbed, the available oxygen molecules needed to convert CO into CO_2 is reduced, lowering CO conversion. After absorption comes release of oxygen from the honeycomb into the exhaust gas. This excess of oxygen molecules then greatly improves the conversion efficiency of CO into CO_2. As discussed in the literature review, forced dithering of the controller on the EGO set point may help improve the dithering of post-catalyst CO levels. Significant future work would be instructive to find the correct amplitude, wave length and wave type to flatten the post-catalyst CO curve. However, since the NO_x and CO appears to have different wave lengths optimizing, the controller to flatten the CO curve may cause detrimental effects on the NO_x curve.

Another result of performing this additional testing showed that the EGO sensor is not always consistent. In each of the three repeated test points the engine was operating at the same speed and power and therefore, the fuel valve would be expected to be in nearly the same position to give a repeated air-to-fuel ratio. The valve however was placed in a different position by the controller due to the EGO reading in all but one of the repeated tests. Further study and examination of the EGO sensor is warranted from this data to discover exactly what is causing the variation in the valve position.

Fuel Flow Test Results

The next test result obtained was the fuel flow rate from the supplemental fuel supply line. Table 5.4 shows two test points at 1,600 rpm.

Table 5.4 Fuel Flow Test

Speed (rpm)	Discharge Pressure (psig)	Engine Fuel Flow (lb/min)	Compressor Flow (lb/min)	Torque ($ft\text{-}lb_f$)	BSFC (BTU/bhp-hr)	Thermal Efficiency	Brake Power (hp)
1602.5	71.09	**0.249**	8.921	78.8	**0.622**	**0.212**	24.1
1601.7	71.39	**0.237**	8.947	79.4	**0.585**	**0.225**	24.2
1601.7	71.39	**0.249**	8.947	79.4	**0.615**	**0.214**	24.2

The first row shows the test results with the supplemental fuel flow turned off, the second row shows the results with the supplemental fuel flow turned on. Since power and speed are essentially the same at both test conditions, the difference in the two measured fuel flow rates represents the supplemental fuel flow rate. Equation (5.1), the equation for thermal efficiency demonstrates why.

$$\dot{m} = \frac{\dot{W}_b}{\eta_{th} LHV} \tag{5.1}$$

In the two test cases, the brake power and fuel used were the same, therefore equation (5.1) indicates that the mass flow rate of fuel and thermal efficiency differ between the two test points. However, since the thermal efficiency should remain constant for a repeated test point, the fuel flow rate must be understated, which is also known to be true due to the closing of the supplemental fuel flow line. By subtracting the two fuel flow rates as seen in equation (5.2), the amount of supplemental flow is calculated.

$$\dot{m}_1 - \dot{m}_2 = 0.249 \frac{\text{lb}}{\text{min}} - 0.237 \frac{\text{lb}}{\text{min}} = 0.012 \frac{\text{lb}}{\text{min}} \tag{5.2}$$

By increasing the fuel flow rate in the second test by 0.012 pounds per minute, the thermal efficiency and BSFC can be recalculated on row three and the values match nearer to the initial values.

The similar results were found for testing at all three engine speeds. Since the GasJack engines operate with the valve opened during field operation, all other testing was preformed with the supplemental valve opened. The measured fuel flow rate was increased by 0.012 pounds per minute to account for the supplemental fuel flow.

Engine and NSCR Characterization

After performing the engine testing, graphs of speed versus engine performance were made to verify the engine was operating consistently, and the data was repeating itself. These graphs characterize or map the engine's performance.

Figure 5.6 shows a plot of brake horsepower vs. speed.

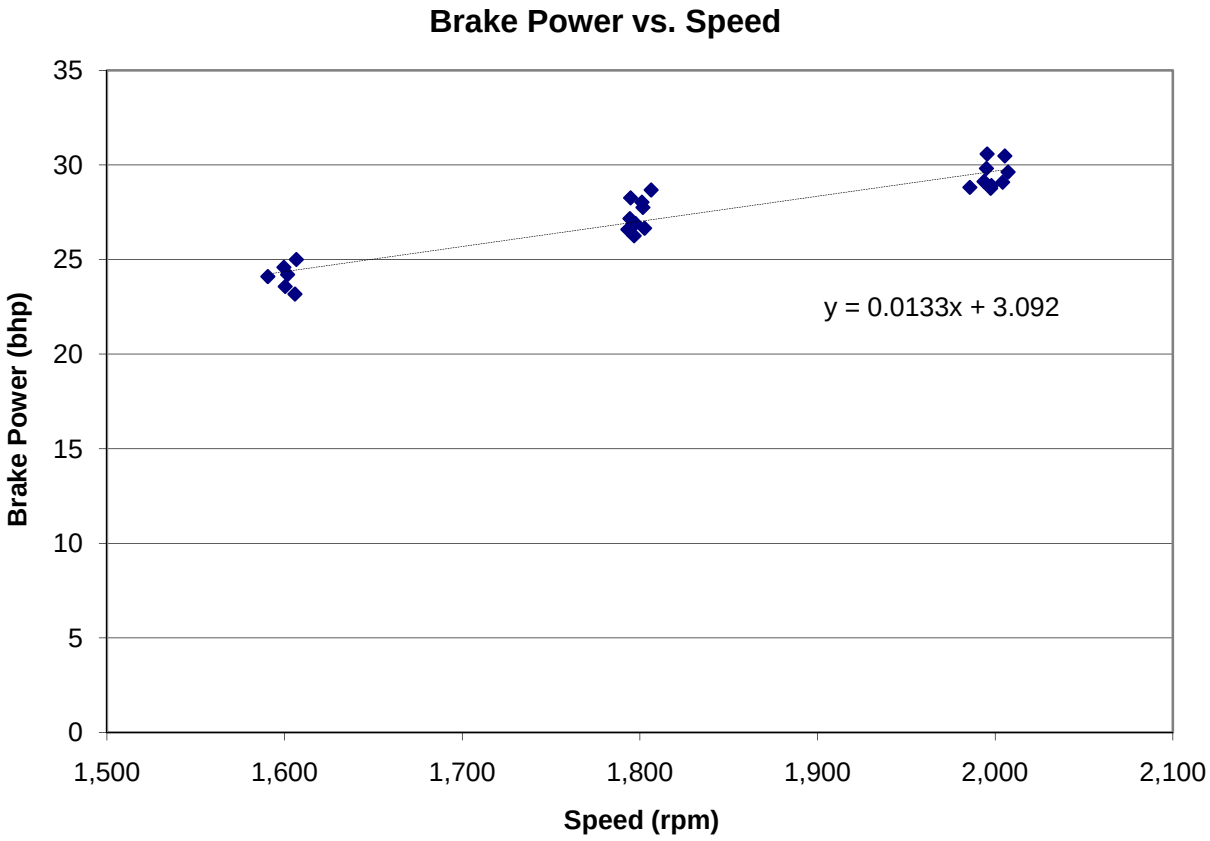

Figure 5.6 Brake Power vs. Speed

This figure shows data points throughout the speed range of 1,600 to 2,000 rpm and shows that the power consumed by the compressor increased with speed. The power measurement was performed on the compressor side of the engine. On an integral engine, gas industry standards typically estimate five percent loss. That means for all given power data, the engine is producing five percent more according to industry estimates. However, the delivered horsepower to run the compressor is the value used in emission reduction and therefore that figure is used as brake power throughout the rest of this thesis. All the points taken at each speed show the same trend. This increase in power with speed is observed because the engine produced near constant torque at all conditions during engine testing.

Figure 5.7 is a plot of engine torque vs. speed.

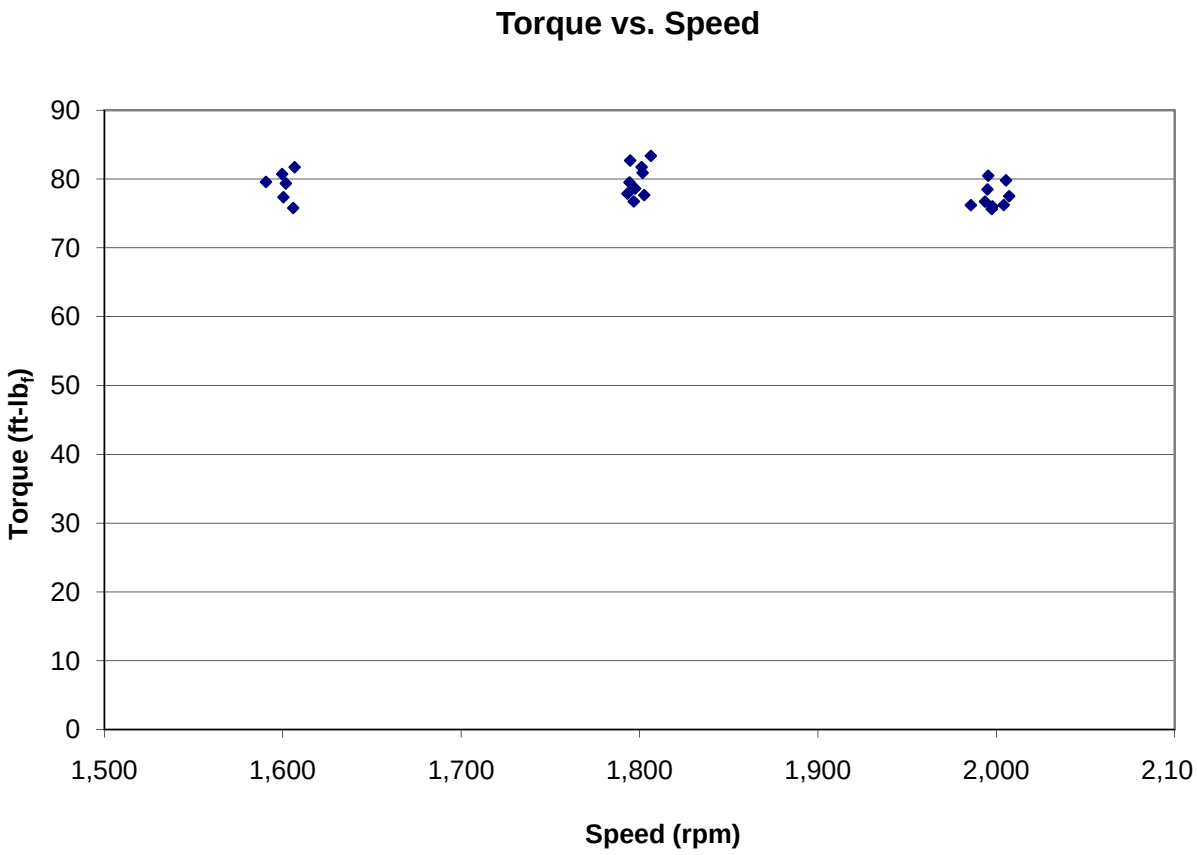

Figure 5.7 Torque vs. Speed

Engine torque is typically measured by a dynamometer in engine testing and power is calculated from torque. In this testing though, compressor power was calculated first and torque was determined from power. Testing showed that the engine produced a near constant torque at all three speeds and compressor discharge pressures.

In Figure 5.8, BSFC vs. Speed is graphed.

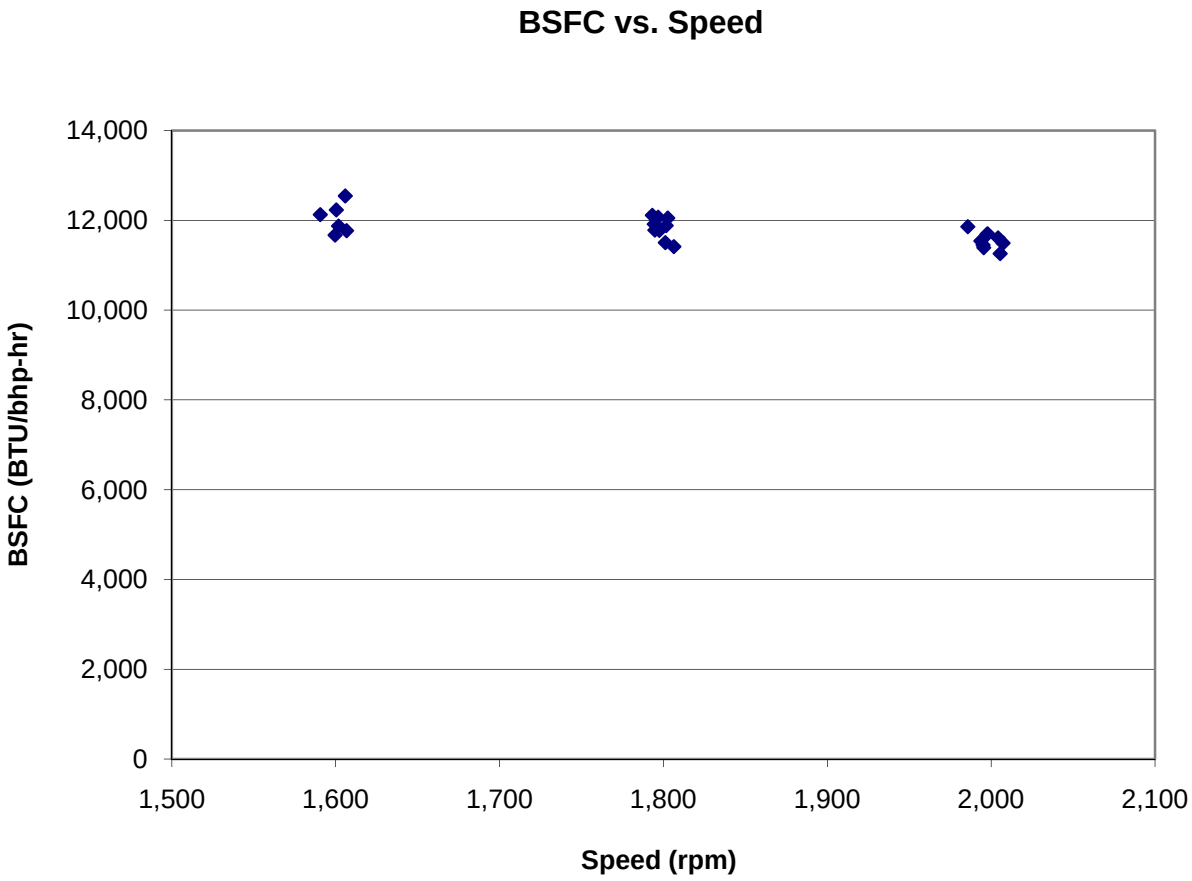

Figure 5.8 BSFC vs. Speed

The brake specific fuel consumption is a measure of the amount of fuel consumed per horsepower for one hour. In the gas industry, BSFC is typically reported in BTU/hp-hr instead of lb_m/hp-hr. This is done by multiplying the BSFC calculation by the lower heating value of the fuel. BSFC is a measure of engine efficiency. For a given engine, lowering the BSFC increases the thermal efficiency. In testing it was found that the BSFC decreased slightly at higher speeds which indicated the engine operates more fuel efficiently at higher speeds.

Figure 5.9, Figure 5.10, Figure 5.11 and Figure 5.12 show brake specific engine emissions as a function of engine speed. These figures show specific emissions before and after the catalyst, so the figures show pre- and post-catalyst levels along with the catalyst efficiency.

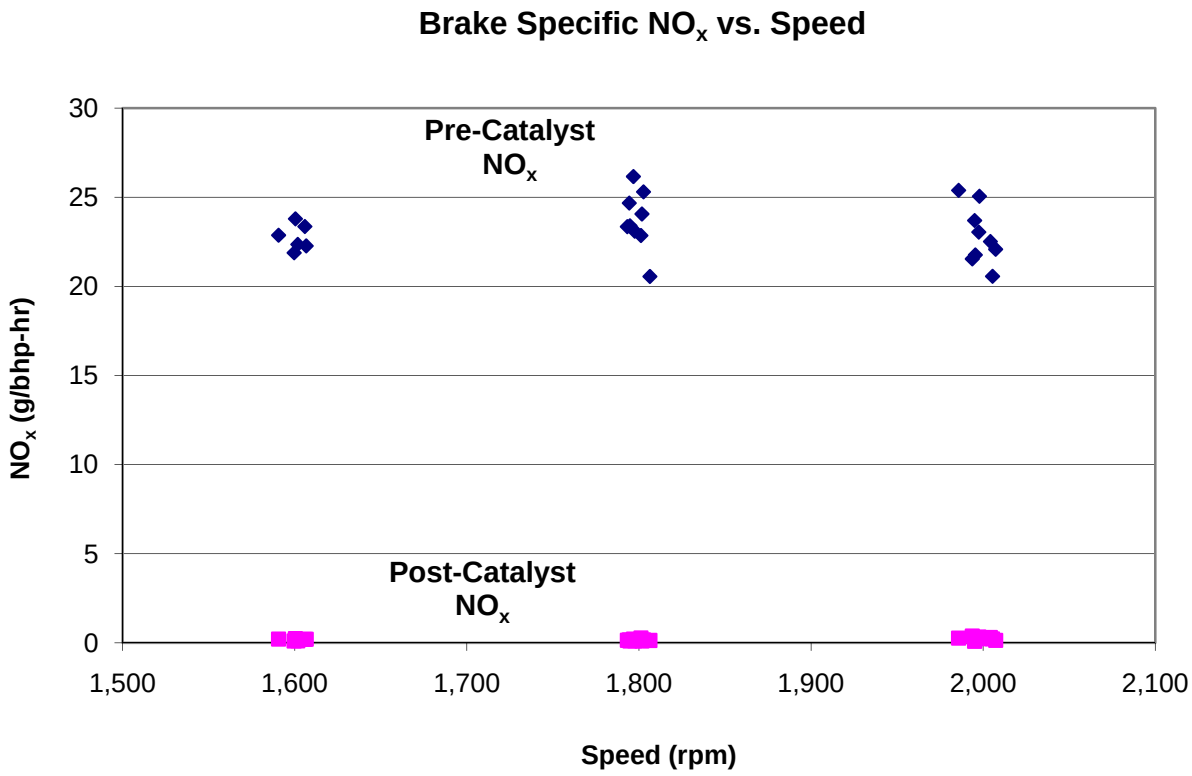

Figure 5.9 Brake Specific NO_x vs. Speed

During testing, the pre-catalyst and post-catalyst brake specific NO_x emissions remained nearly constant throughout the engine speed range. Pre-catalyst NO_x levels averaged 23.1 g/bhp-hr, while post-catalyst NO_x emissions were on average 0.2 g/bhp-hr. From these values it was found that the catalyst conversion efficiency for NO_x was always greater than 99% throughout the engine speed range. This can be clearly seen in Figure 5.10.

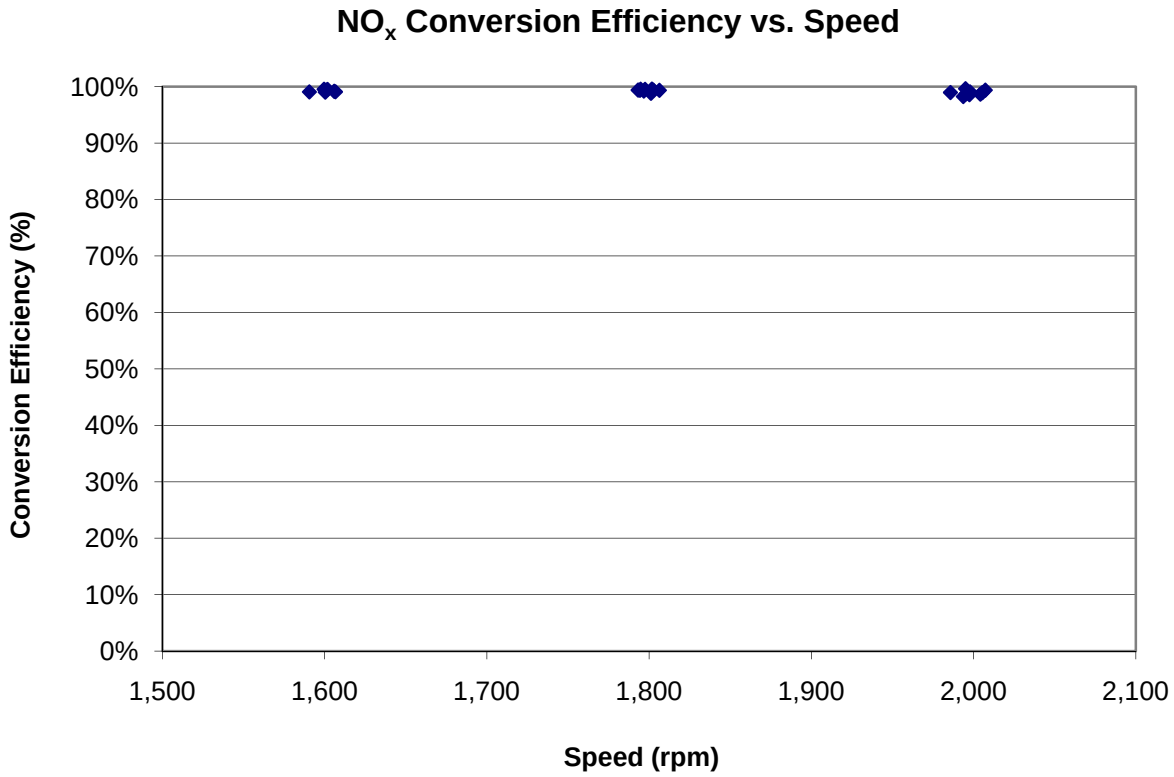

Figure 5.10 NO_x Conversion Efficiency vs. Speed

Conversion of NO_x was 99.2% on average for all test points. This high NO_x conversion efficiency indicates that the controller and catalyst are well suited for reducing NO_x levels. Additionally this very high conversion efficiency indicates that the set point of the controller may have been set too rich. By recalling Figure 2.6 the data shows that there is a tradeoff between NO_x and CO conversion efficiency. When NO_x conversion efficiency is high, like seen here, CO conversion efficiency will be reduced. In this testing NO_x efficiency was high, consequently optimizing NO_x reduction at greater efficiency than CO.

Figure 5.11 shows brake specific CO vs. speed before and after the catalyst.

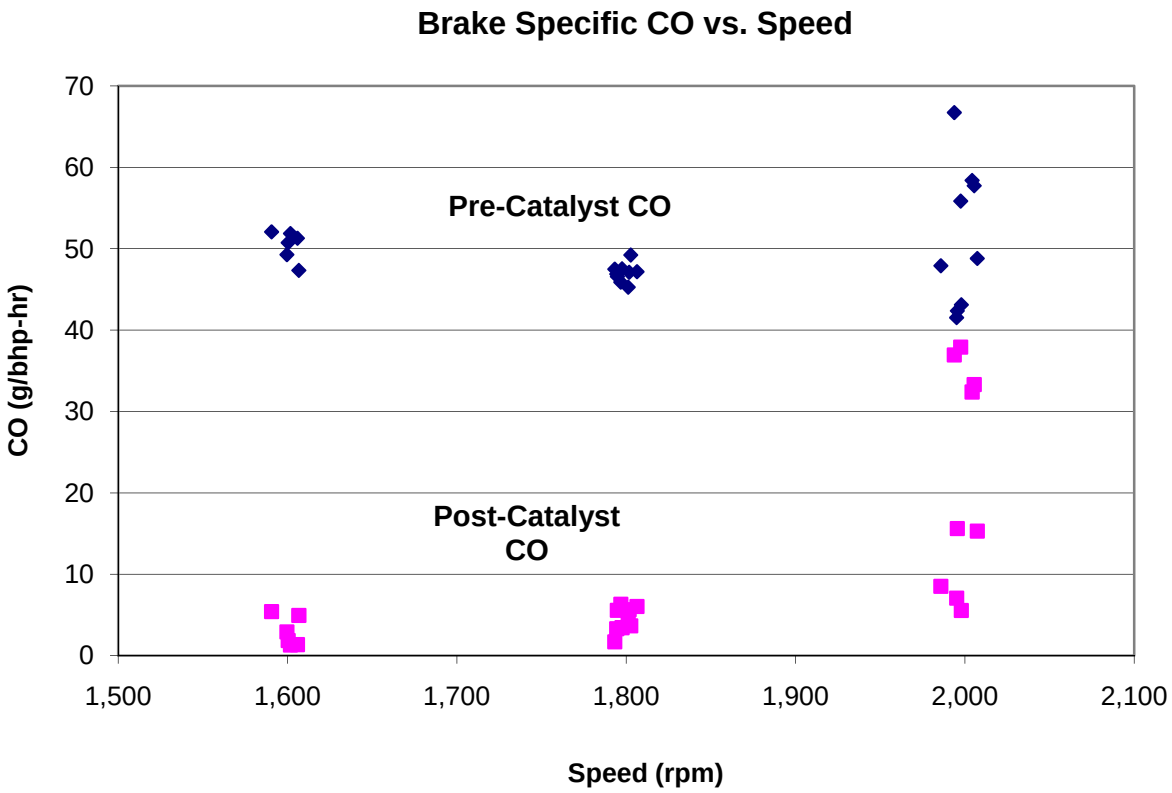

Figure 5.11 Brake Specific CO vs. Speed

The data shows that at 1,600 and 1,800 rpm the data points are closely grouped while at 2,000 rpm the data points for both pre- and post-catalyst levels have a significant amount of scatter. This is different than what was found for NO_x. The data, in addition to scattering, showed a decline in catalyst conversion efficiency at 2,000 rpm.

Figure 5.12 shows the conversion efficiency of CO plotted against speed.

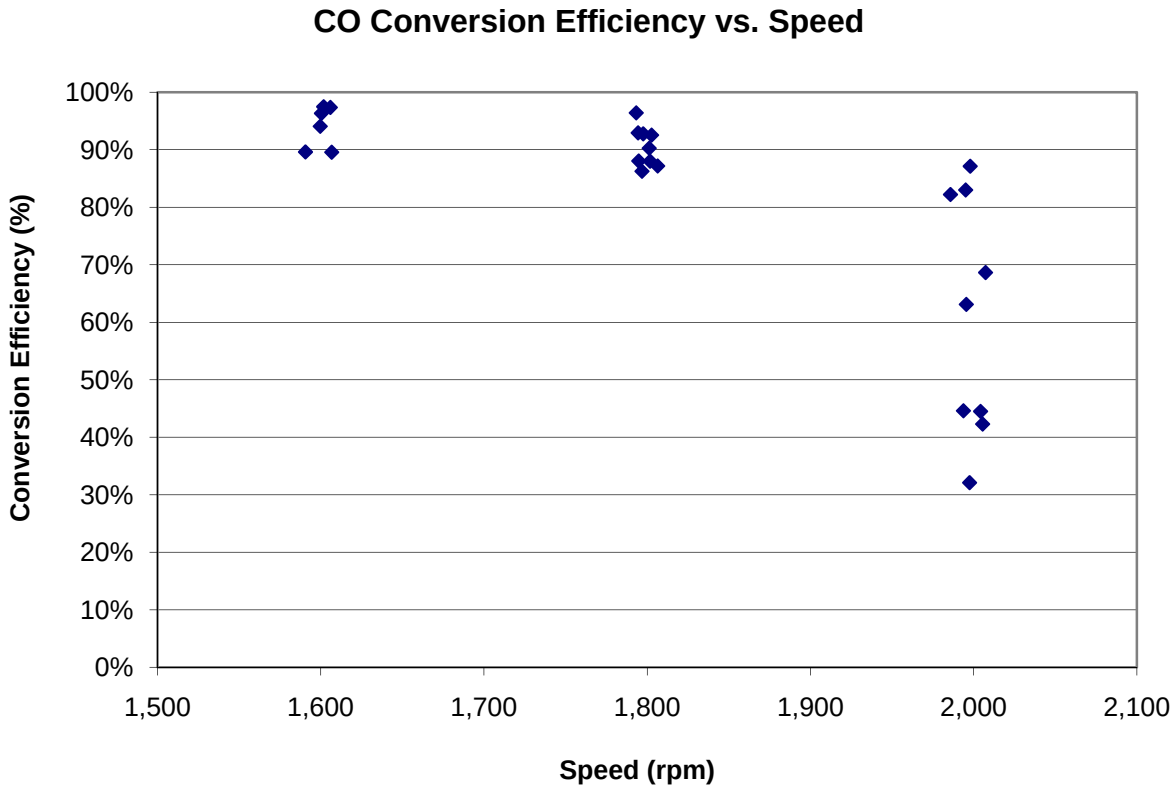

Figure 5.12 CO Conversion Efficiency vs. Speed

For 1,600 and 1,800 the conversion efficiency for CO averaged 92 percent. While this is lower than the 99.2 percent observed for NO_x, it is enough to bring pre-catalyst CO emissions from 48.6 to 3.8 grams per horse-power hour. At 2,000 rpm, the conversion efficiency ranges from as high as 87.1 percent to as low as 32.1 percent. The test points which exhibited the worst conversion efficiency were at the full compressor discharge pressure of 90 psig.

Figure 5.13 shows the nine test points at 2,000 rpm from Figure 5.12.

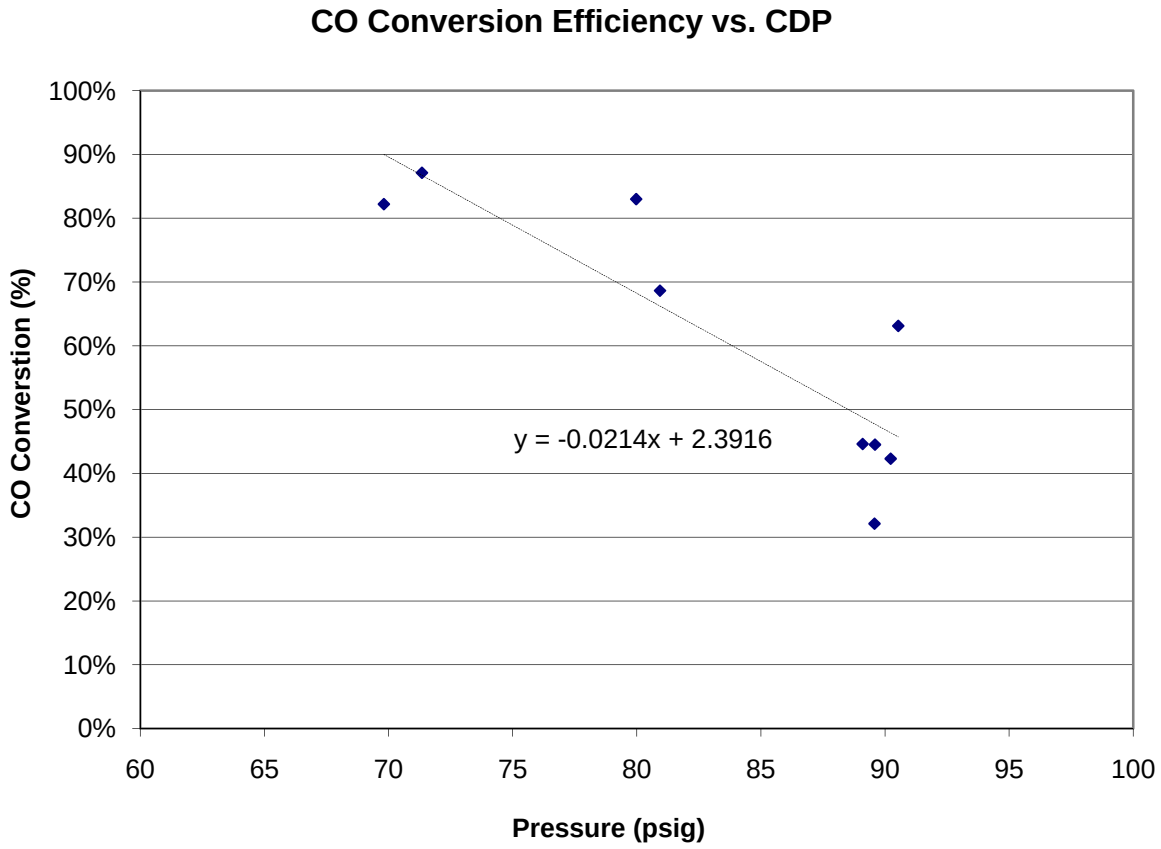

Figure 5.13 CO Conversion Efficiency vs. Compressor Discharge Pressure

Figure 5.13 shows that it is not only the engine speed which causes the CO levels to be high, but a combination of maximum speed and maximum compressor discharge pressure (CDP). The effects of speed and CPD on the ability of the AFRC and NSCR system to control the emissions are explored next.

Figure 5.14 through Figure 5.17 show the relationship between power and brake specific emissions.

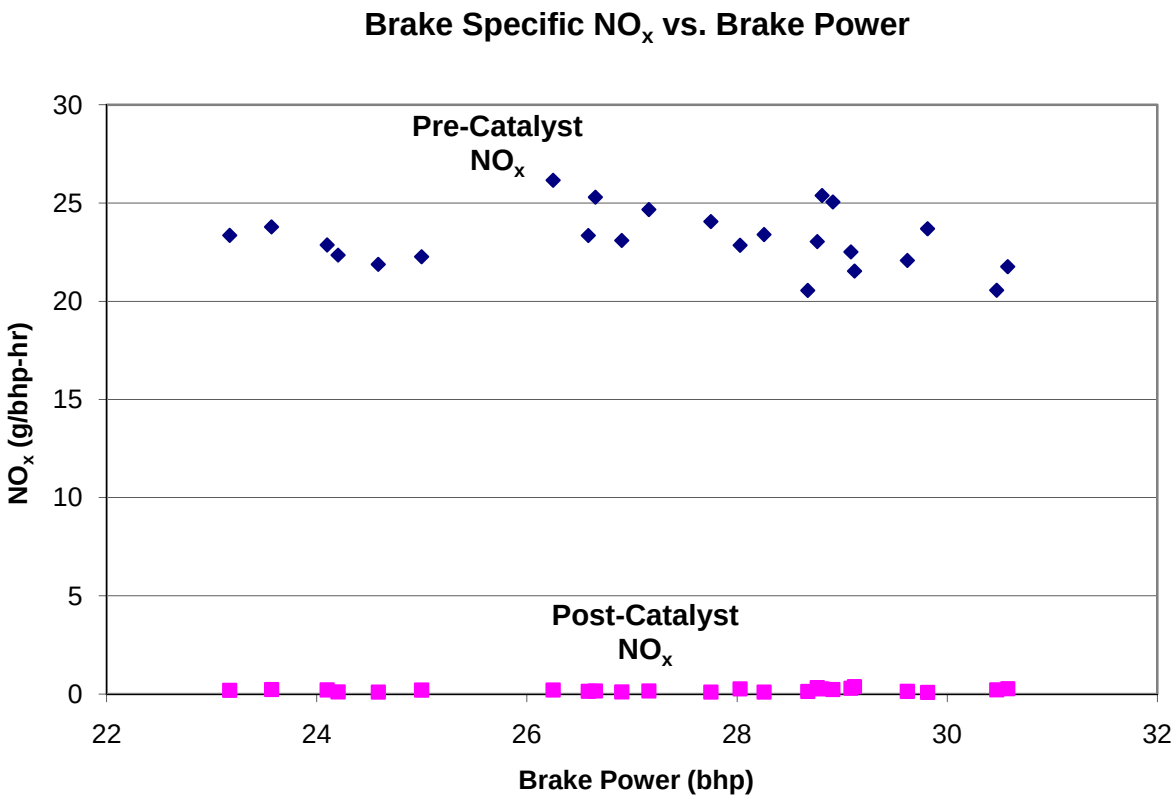

Figure 5.14 Brake Specific NO_x vs. Brake Power

Figure 5.14 agrees with Figure 5.9, they both indicate nearly constant levels of brake specific NO_x both before and after the catalyst. Constant brake specific NO_x is found throughout all speed ranges and brake power levels.

Figure 5.15 shows the conversion efficiency of NO_x vs. power and once again the trend agrees with what was seen in relationship of speed and conversion efficiency for NO_x.

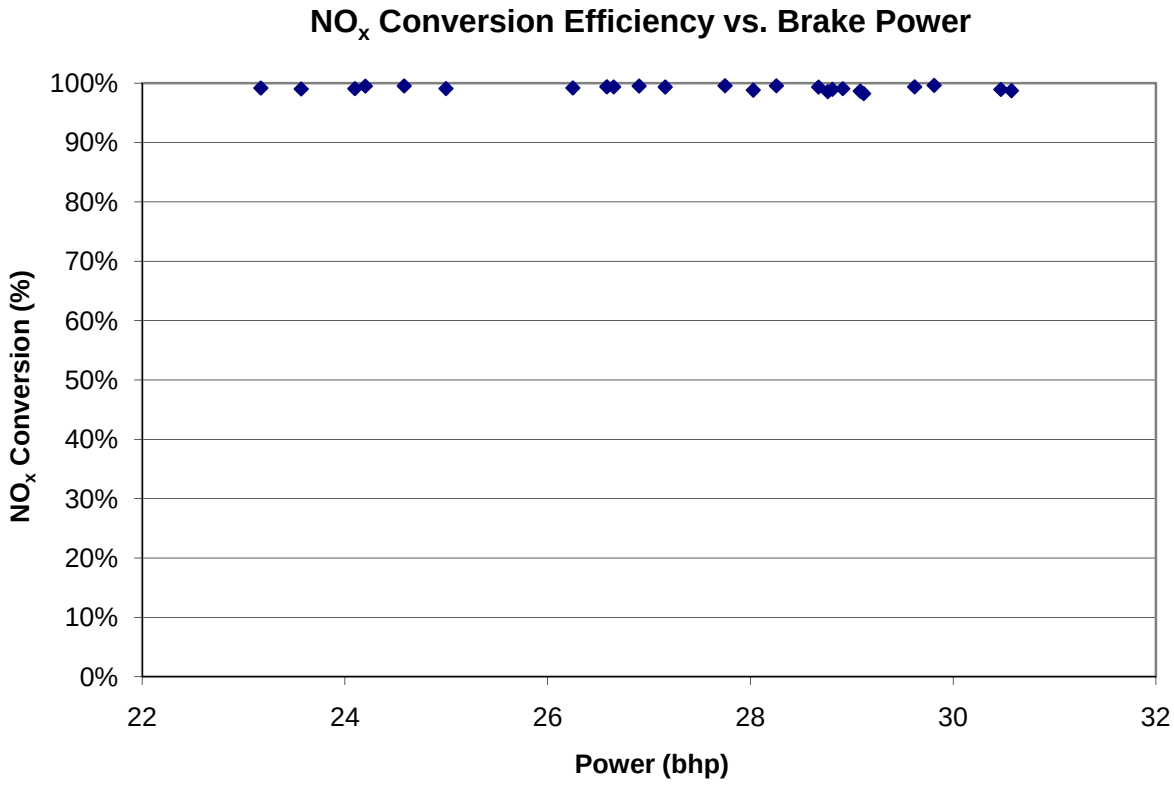

Figure 5.15 NO_x Conversion Efficiency vs. Brake Power

The next two figures are of brake specific CO and CO conversion efficiency plotted against power. Figure 5.16 shows the relationship between brake specific CO and power for pre- and post-catalyst emissions.

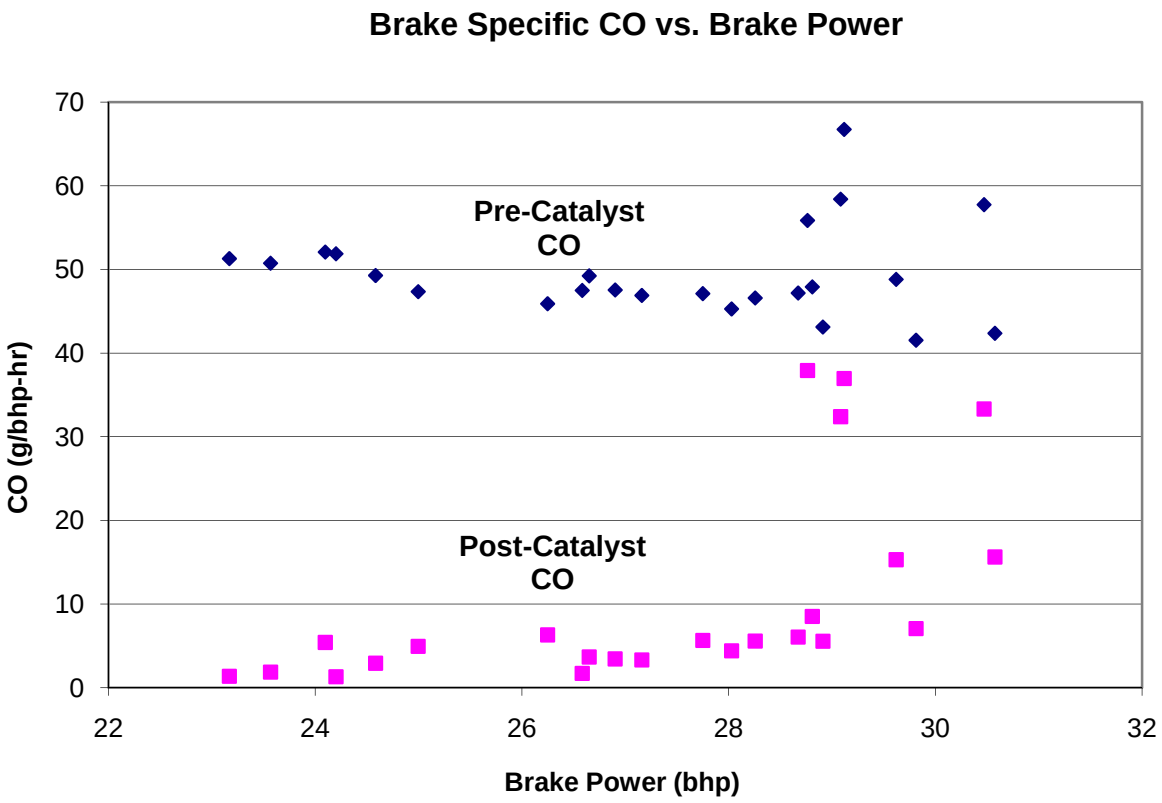

Figure 5.16 Brake Specific CO vs. Power

The brake specific CO at horsepower's less than 29 were much more constant and consistent than CO emissions at the upper power range. By referencing back to the graph of power versus speed (Figure 5.6), the data shows that horsepower levels at or above 29 hp were achieved on the 2,000 rpm speed line. When taking that into account, the scattered data points above 29 hp are the same as the scattered data points at 2,000 rpm in Figure 5.11 and Figure 5.13.

Figure 5.17 plots CO conversion efficiency vs. power.

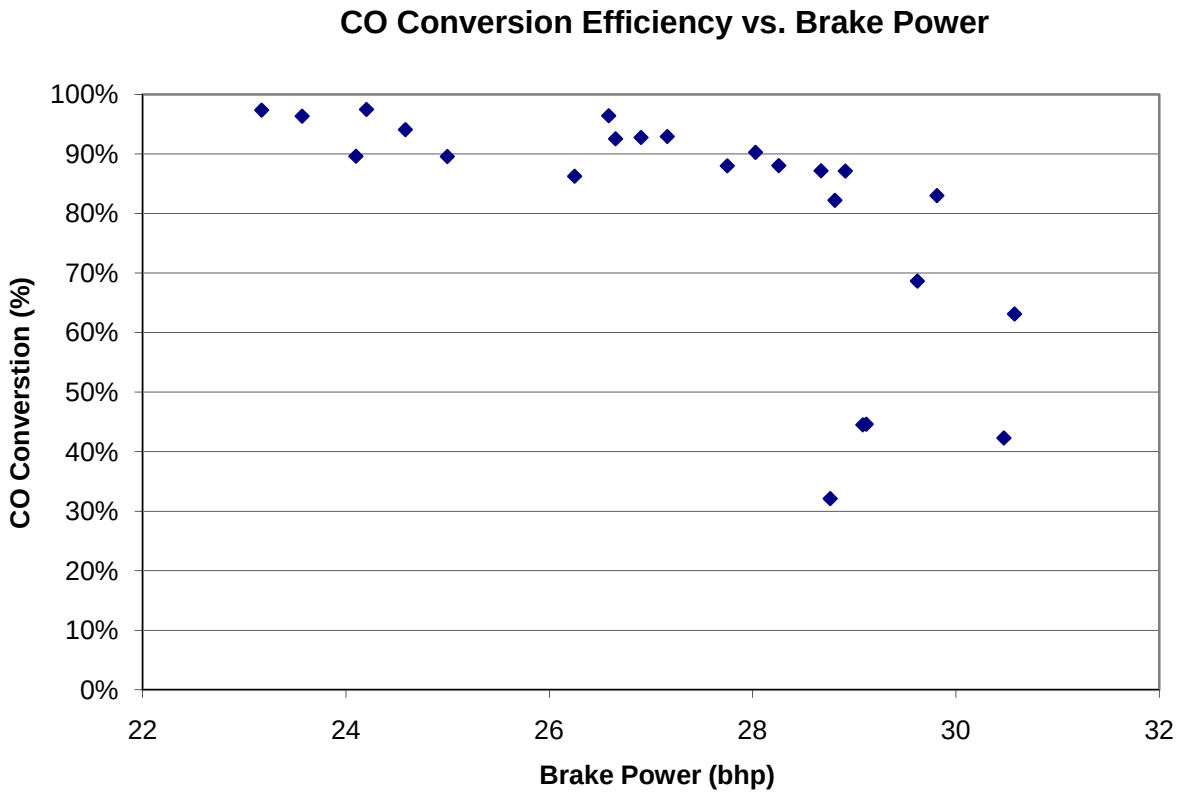

Figure 5.17 CO Conversion Efficiency vs. Brake Power

This data also shows that at 29 hp, the conversion efficiency begins to decline. To explore why the AFRC loses ability to convert CO at a high efficiency at maximum speed and power, the pre-catalyst oxygen level was examined to determine if a correlation existed.

Figure 5.18 shows the relationship between pre-catalyst oxygen concentration and power.

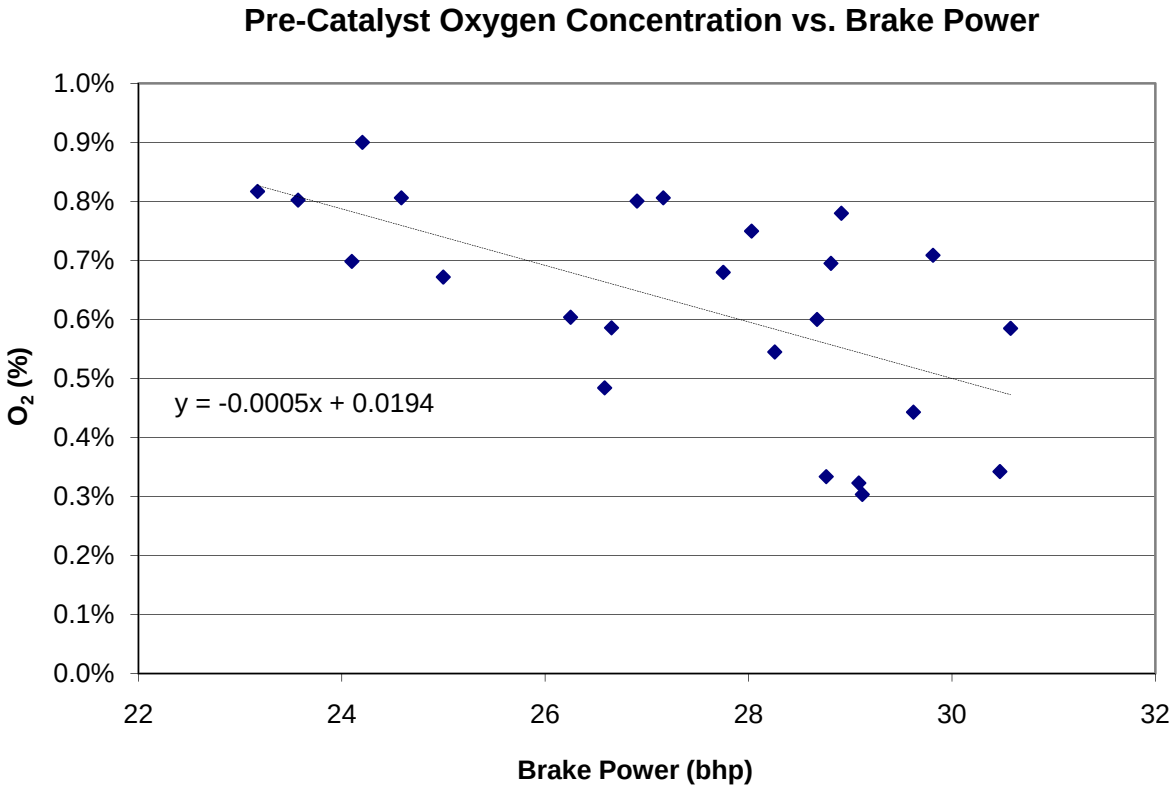

Figure 5.18 Pre-Catalyst Oxygen Concentration vs. Brake Power

While there is some scatter of the data points, a trend towards less oxygen at higher power levels is observed. The oxygen concentration measured in percent has an uncertainty of 0.1% which could cause this trend to be over or understated. For a better look at this same data, pre-catalyst oxygen levels have been plotted against speed in Figure 5.19.

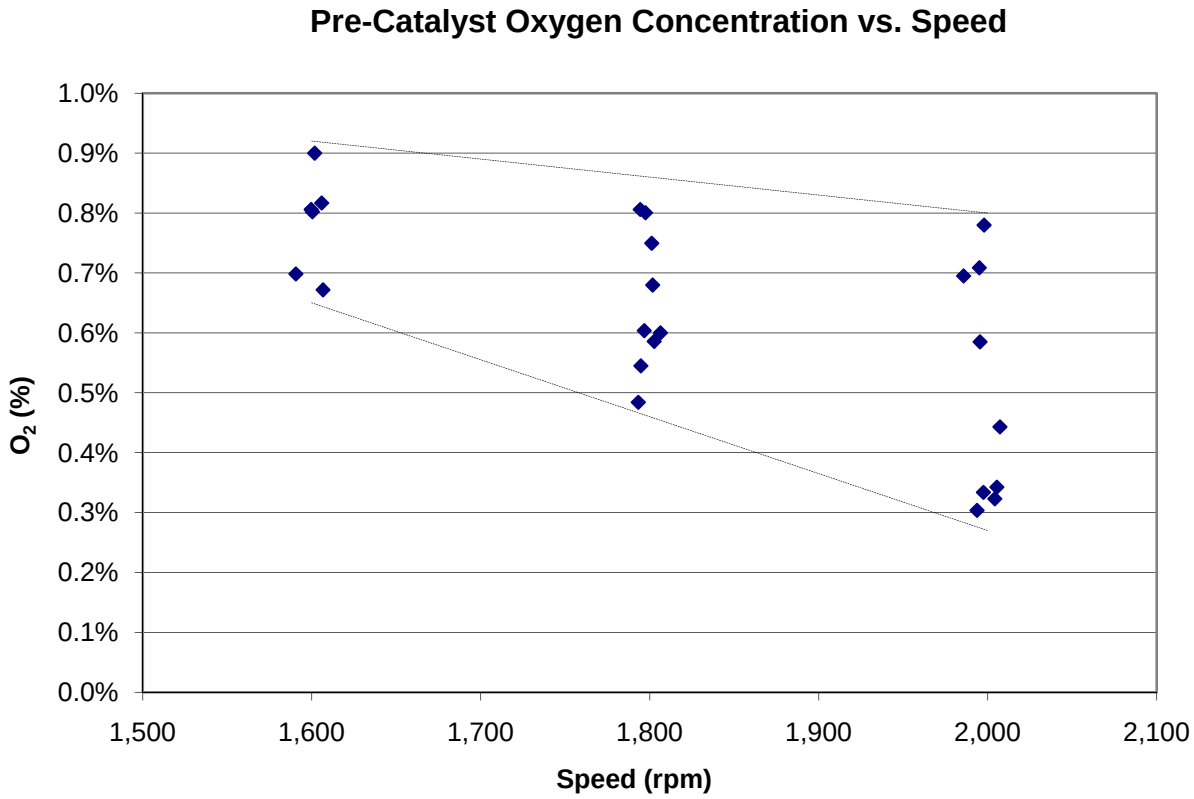

Figure 5.19 Pre-Catalyst Oxygen Concentration vs. Speed

Once again the trend is downward for pre-catalyst oxygen concentration as speed increases. More interestingly though is that the points widen considerably at 2,000 rpm compared to 1,600 rpm. In fact, when considering the uncertainty of 0.1%, all the points at 1,600 rpm can be considered to be the same, but because of the range of 0.3% to 0.8% at 2,000 rpm there is a definite spread of the data observed at 2,000 rpm. These two figures indicate that it is not actually the high speed, high CPD, or high power levels that are causing a decline in the CO conversion efficiency but a lack of pre-catalyst oxygen at those conditions. The controller was unable to keep sufficient oxygen levels at high speeds and powers. The reason for the controller failing to accurately and precisely maintain the correct oxygen concentration at increased speed and power is not clear. One plausible explanation is the oxygen sensor is being influenced adversely at these speeds and powers; this could worsen the already suspected inconsistencies and inaccuracies of oxygen sensor. Recall Figure 5.12 CO Conversion Efficiency vs. Speed, at 2,000 rpm the data was scattered similar to the ones seen in Figure 5.19.

By plotting specific emissions and catalyst conversion efficiency against pre-catalyst oxygen level instead of speed or power, a better understanding of magnitude of the conversion was obtained. Figure 5.20 plots brake specific CO both before and after the catalyst against pre-catalyst oxygen concentration.

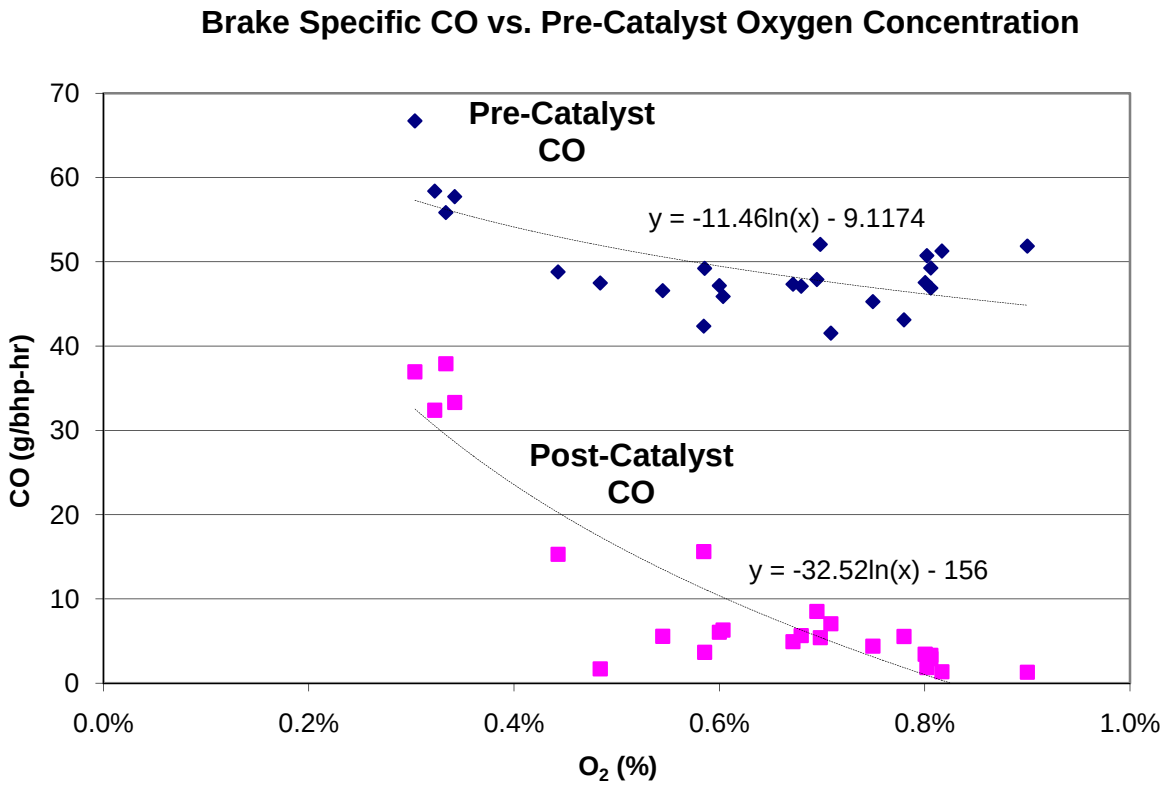

Figure 5.20 Brake Specific CO vs. Pre-Catalyst Oxygen Concentration

The data in this figure shows that as the oxygen concentration before the catalyst decreases the CO increases. Decreasing oxygen levels indicate that the engine is running richer. By recalling Figure 2.3, it shows that CO does, in-fact, increase as the combustion process richens. Additionally from the literature, Figure 2.6 specifically, it is known that as an engine runs richer than the perfect AFRC set point, the catalyst becomes less effective at converting CO.

Figure 5.21 shows the conversion efficiency of CO plotted against pre-catalyst oxygen concentration.

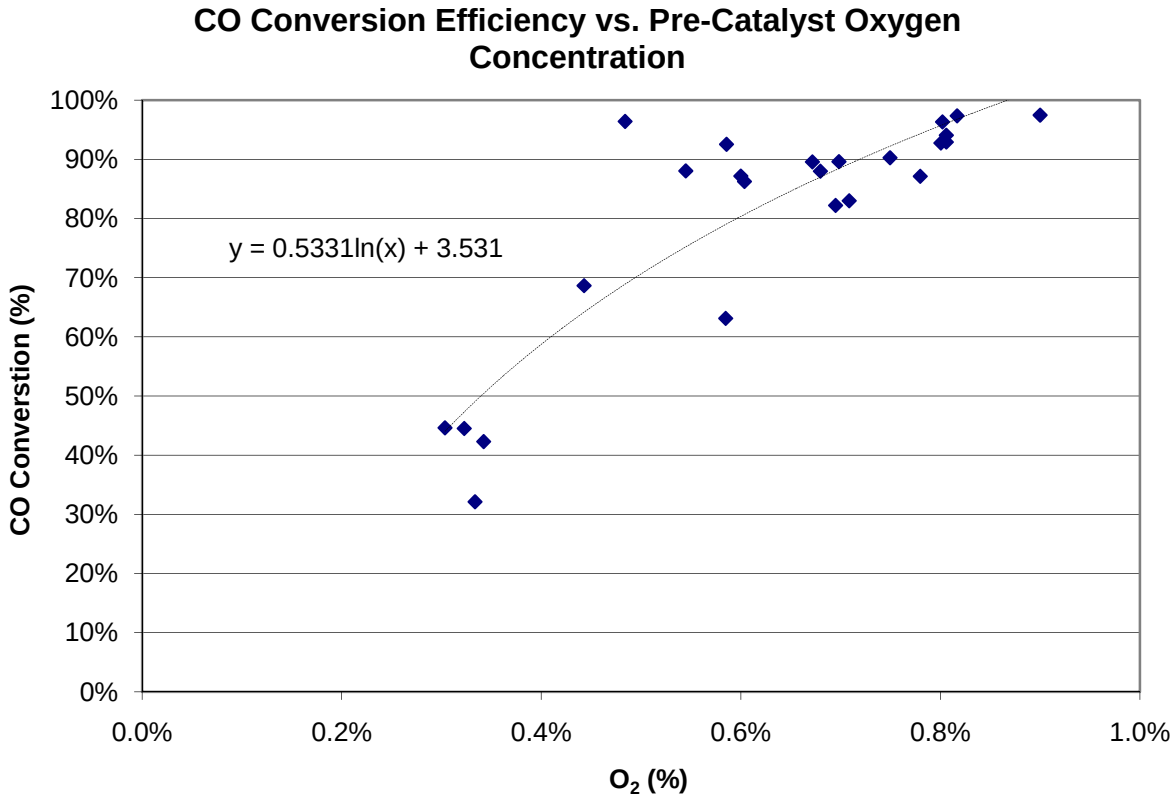

Figure 5.21 CO Conversion Efficiency vs. Pre-Catalyst Oxygen Concentration

The trend line in Figure 5.21 agrees with the curve for CO observed in Figure 2.6. Once again the four points with conversion efficiency below 50% are the points taken at maximum speed and CDP. The CO conversion efficiency, the pre-catalyst CO values and the pre-catalyst oxygen concentrations all indicate that the engine is operating richer at those four points. While decreases of 0.1% are due to small changes in the air-to-fuel ratio, a difference of 0.1% is equal to 1,000 ppm of O_2. Since pre-catalyst CO concentrations ranged from 12,000 ppm to 18,000 ppm 0.1% of O_2 greatly increases the amount of O_2 which was available to convert the CO molecules into CO_2.

For completeness Figure 5.22 and Figure 5.23 show brake specific NO_x vs. pre-catalyst oxygen concentration and NO_x conversion efficiency vs. pre-catalyst oxygen concentrations respectively.

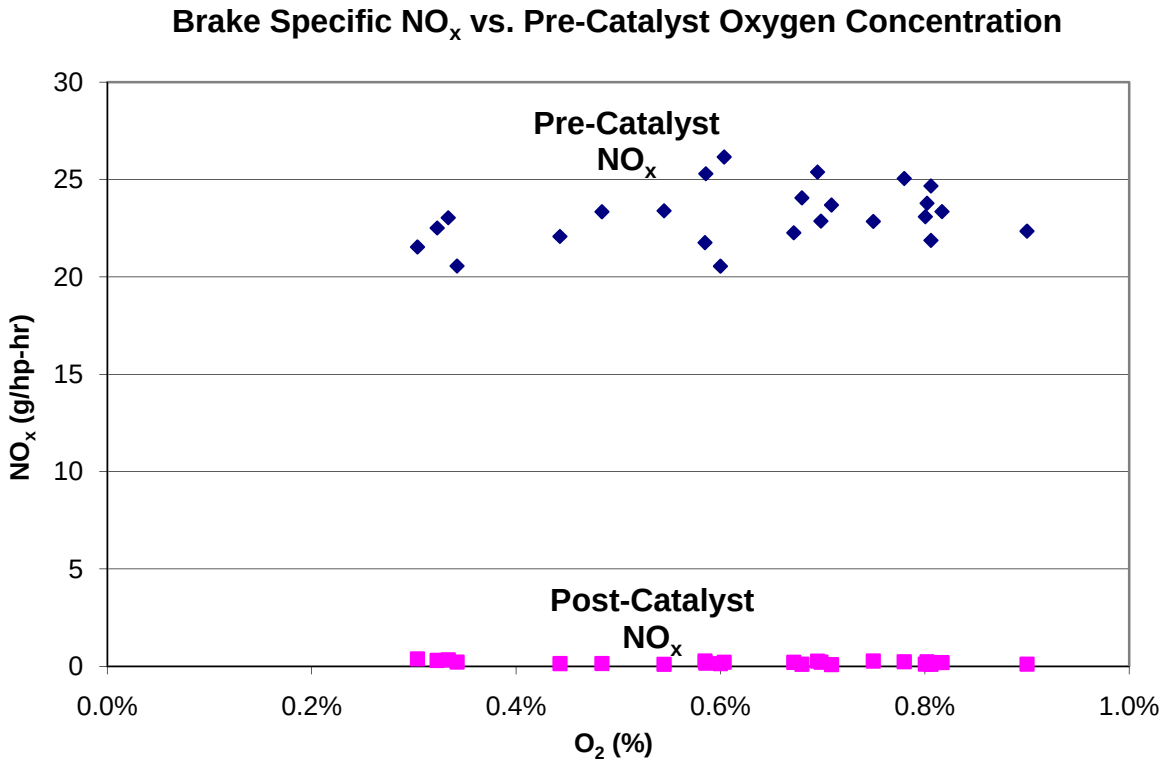

Figure 5.22 Brake Specific NO_x vs. Pre-Catalyst Oxygen Concentration

The specific NO_x emissions both before and after the catalyst remain nearly constant for all pre-catalyst oxygen levels. This indicates that the formation of NO_x is not as dependent on air-to-fuel ratio as is CO. This agrees with what was found in the literature. NO_x is a function of temperature and time, while CO is a function of air-to-fuel ratio (Heywood, 1988).

Figure 5.23 shows a graph of NO_x conversion efficiency vs. pre-catalyst oxygen concentration.

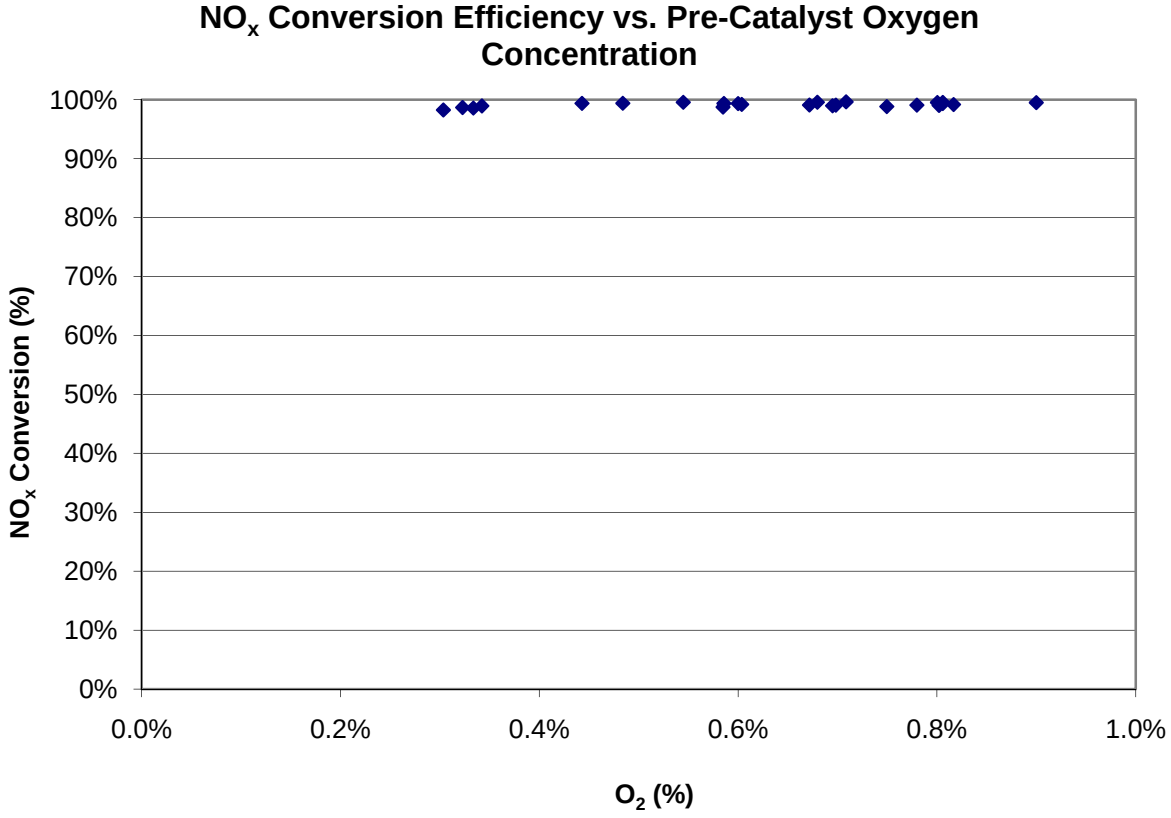

Figure 5.23 NO_x Conversion Efficiency vs. Pre-Catalyst Oxygen Concentration

The data in Figure 5.23 shows that the catalyst conversion efficiency of NO_x was nearly 100% for all pre-catalyst oxygen levels. From the literature it was expected that the conversion of NO_x would only be near 100% under rich of stoichiometric engine operating conditions. This was not the case, it was found that even at oxygen levels as high as 0.8% to 0.9% the conversion efficiency remained high. One reason could be that when NO_x conversion efficiency does begin to decline it does so along a steep curve. It is possible that the catalyst remains effective at 0.9% but if more testing was done at higher pre-catalyst oxygen levels, NO_x catalyst conversion efficiency could begin to drop off sharply for each additional 0.1%.

CHAPTER 6 - Conclusions

After testing and data analysis, the results indicate that the catalyst is highly effective at converting NO_x at all speeds and powers. The catalyst also exhibited a sufficient CO conversion efficiency at lower engine speeds and powers, but failed at maximum power and speed. The failure of the NSCR system to convert CO at a high level under all test conditions was due to the AFRC systems inability to keep pre-catalyst oxygen concentrations at high enough levels. The problem however, is not entirely with the controller. One major reason the controller failed is due to an inaccurate or inconsistent sensor. A summary of the key findings are:

- The small supplemental fuel flow found on all Compressco GasJack engines is not large enough to affect the ability of the AFRC system;
- Pre-catalyst emission concentrations of NO_x were consistent from 1,600 to 2,000 rpm and at all and powers;
- Post-catalyst emission concentrations of NO_x were consistent at all speeds and powers;
- The catalyst conversion efficiency of NO_x was greater than 99% in all testing;
- Pre-catalyst emission concentrations of CO increased at high speeds and powers due to decreased air-to-fuel ratio;
- Post-catalyst emission concentrations of CO highly depended on pre-catalyst oxygen concentration;
- Post-catalyst emission concentrations of CO fluctuated under steady state conditions:
    - Fluctuation, or dithering, remained evident with the AFRC off
    - Dithering is due to the natural storage and release of oxygen, not from real time adjustment by the controller
- The catalyst conversion efficiency of CO was dependant on pre-catalyst oxygen concentration;
    - When the pre-catalyst oxygen concentration was in the range of 0.7% to 0.9%, the conversion efficiency was above 90%

    - When the oxygen concentration decreased below 0.7% conversion efficiency declined sharply
- The catalyst exhibited maximum conversion efficiency for both NO_x and CO when pre-catalyst oxygen concentration was between 0.7% and 0.9%;
- The air-to-fuel ratio controller performed well at keeping the oxygen sensor output at the desired set point of 777 mV;
- The output of the oxygen sensor is not perfectly correlated to oxygen concentration.
    - This is seen by comparing the measured oxygen concentration which ranges from 0.3% to 0.9% while the oxygen sensor output remained at 777 mV
    - Increased pre-catalyst CO concentration is evident of a richer air-to-fuel ratio, while the oxygen sensor output remained at 777 mV
    - The AFRC placed the fuel control valve in different positions to keep the oxygen sensor output at 777 mV on repeated identical test points

In comparison with the literature, the test findings were consistent with what others have found. Table 6.1 shows a comparison of the catalyst efficiency and the best operating point.

Table 6.1 Test Results and Compairson with the Literature

	Test Findings	**Defoort et al., 2004**	**Lambert, 1995**	**Kennedy and Holdeman, 2006**	**Emit, 2007**
Optimal Engine Operating Point	0.7 – 0.9% O_2	ϕ=1.013 – 1.027	< 0.5% O_2	0.2 – 0.7% O_2	0.25 – 0.5% O_2
NO_x Efficiency	99%	80%	98%	-	90%
CO Efficiency	90%	80%	98%	-	80%

The 90% CO conversion efficiency in the test findings column does not include those points taken where the controller had obviously failed to keep pre-catalyst oxygen levels in the correct range. By comparing only results where the NSCR system was functioning correctly, it was

found that NO_x efficiency was very high at 99%, and CO efficiency was also very good at 90%. It was also found that the optimal oxygen content was slightly higher in this testing than what others had found in their tests.

In summary, the addition of an NSCR and AFRC system can reduce emissions of NO_x and CO when the pre-catalyst oxygen concentrations are accurately controlled. The AFRC was able to control the output of the oxygen sensor at all test points. However, the gas analyzer showed that a given oxygen sensor output didn't not yield a repeatable pre-catalyst oxygen concentration. Recommendations for further work include:

- Study of the oxygen sensor to understand the meaning of the sensor output;
- Improve the accuracy of the oxygen sensor so that the output has a direct relation with oxygen concentration; or
- Development of an economical and robust sensor which accurately measures oxygen concentration.

References

3-Way Non-Selective Catalytic Reduction (NSCR) deNOx Catalyst. (2007). http://ect.jmcatalysts.com/applications-ssec-na-products-nscr.htm

Agrawal, A., K., Singh, S., K., Sinah, S., & Shukla, M., K. (2004). Effect of EGR on the Exhaust Gas Temperature and Exhaust Opacity in Compression Ignition Engines. *Sadhana,*

Arney, G., McGivney, D., Beshouri, G., & Ashon, G. (2007). Detection of Excess Emission Conditions for Rich Burn Engines Equipped with Non-Selective Catalytic Reduction Systems Operating at California Best Available Control Technology Limits. Paper presented at the *Gas Machinery Conference,* Dallas, TX.

Bathie, W. W. (1996). *Fundamentals of Gas Turbines* (2nd ed.). New York, NY: John Wiley & Sons, Inc.

Beshouri, G., Willson, B., & Chapman, K. S. (2005). *Pipeline Engine Emissions Control Roadmap*

Bevington, P. R., & Robinson, D. K. (2003). *Data Reduction and Error Analysis* (3rd ed.). New York, NY: McGraw-Hill.

Chapman, K. S. (2007). *Field Test Characterization of NSCR Catalysts on Engines used in the Oil and Gas Gathering Industry*

Ciulla, V. T. (2003). *Catalytic Converters*.http://autorepair.about.com/cs/generalinfo/a/aa080401a.htm

Compressco Inc. (2007). *Specifications*.http://www.compressco.com/Specifications.shtml

Cusick, C. F. (1961). *Flow Meter Engineering Handbook* (3rd ed.). Philadelphia, PA: Minneapolis-Honeywell Regulator Company.

Defoort, M., Olsen, D., & Willson, B. (2004). The Effect of Air-Fuel Ratio Control Strategies on Nitrogen Compound Formation in Three-Way Catalysts. *Int. J. Engine Res., 5*(1), 115.

Ely, C. (2004). Emission Data Collection, Calculation, and Interpretation. *Engine Emissions Stack Testing & Analyzer Workshop,* Oklahoma City, OK.

Emit Technologies, I. (2003). *Operation and Maintenance Manual Model EAS-1000T*

Emit Technologies, I. (2007). *Edge NG Air Fuel Ratio Controller Installation, Operation, and Troubleshooting Manual*

40 CFR Pt. 90 - Control of Emissions from Nonroad Spark-Ignition Engines at Or Below 19 Kilowatts, (2007).

Ferguson, C. R., & Kirkpatrick, A. T. (2001). *Internal Combustion Engines* (2nd ed.). New York, NY: John Wiley & Sons.

Four Corners Air Quality Task Force. (2007). *Oil and Gas Reciprocating Internal Combustion Engines*

Francis. (undated). M. A. *Benedict-Webb-Rubin Mark 2 Program*

Heywood, J. B. (1988). *Internal Combustion Engine Fundamentals* (1st ed.). New York, NY: McGraw-Hill.

Kennedy, K., & Holdeman, T. (2006). Application of Full Authority Fuel Control Valve for Non Selective Catalytic Reduction on Large-Bore, Four-Stroke Cycle, Natural Gas Fired Reciprocating Engine. *Gas Machinery Conference,* Oklahoma City, OK.

Lambert, D. C. (1995). Current Design, Operation, Performance, and Costs of 3-Way Catalysts on Stationary Natural Gas Engines. *1995 Fall Technical Conference of the ASME Internal Combustion Engine Division, , 4*(25) 91.

Moran, M. J., & Shapiro, H. N. (2004). *Fundamentals of Engineering Thermodynamics* (5th ed.). New York, NY: John Wiley & Sons, Inc.

Reciprocating Internal Combustion Engine Work Group of the Industrial Combustion Coordinated Rulemaking. (1998). *Definition of "Rich Burn Engine" for the Reciprocating Internal Combustion Engine (RICE) MACT Standard*

Rowell, E. (2007). *A Timeline of the Air Quality Act.*, 2007, from http://www.environmentaldefense.org/documents/2695_cleanairact.htm

Southern California Gas Company. (2007). State-of-the-Art and Development Plans for Non-Selective Catalytic Reduction for Natural Gas-Fired Rich Burn IC Engines. *Advanced Stationary Reciprocating Engines Conference,* Downey, CA.

Tice, J. K. (2007). Exhaust Gas After-Treatment: Catalyst Systems. Paper presented at the *Gas Machinery Conference,* Dallas, TX.

White, F. M. (2003). *Fluid Mechanics* (5th ed.). New York, NY: McGraw-Hill.

Appendix A - Compressco Operating Guide

1. Close the 2” ball valve on the compressor inlet scrubber
2. Hook up a 12V battery to the jumper cables on the Compressco
3. Check oil and antifreeze levels
4. Turn on the main gas valve outside the south door
5. Open the manual ball valve for gas supply to the small engine test cell
6. Go to the Opto22 Compressco strategy
    a. Open electronic fuel valve
    b. Set load valve to wide open (20 mA)
7. Open the gas valve between the pressure regulator and the Compressco
8. While watching the compressor suction gauge, slowly open the 2” ball valve on the compressor inlet scrubber and let in a maximum of 5 psig
9. Open 1” by-pass valve on compressor inlet scrubber
10. Turn start timer to 5 minutes
11. Reset any switches that are extended
12. Press starter button on the side of the control panel
    a. Don’t run the starter for more than 10 seconds
    b. You may need to cycle the fuel valve nearest to the engine
13. Allow engine to warm up
14. Close 1” by-pass valve
15. Adjust the engine speed with the ¼ nut on the governor
16. Use Opto22 to load the compressor